

Effective Temperatures of Low-Mass Stars from High-Resolution H-band Spectroscopy

RICARDO LÓPEZ-VALDIVIA,¹ GREGORY N. MACE,¹ KIMBERLY R. SOKAL,¹ MARYAM HUSSAINI,¹ BENJAMIN T. KIDDER,¹
ANDREW W. MANN,² NATALIE M. GOSNELL,³ HEEYOUNG OH,^{1,4} AURORA Y. KESSELI,⁵ PHILIP S. MUIRHEAD,⁵
CHRISTOPHER M. JOHNS-KRULL,⁶ AND DANIEL T. JAFFE¹

¹*The University of Texas at Austin, Department of Astronomy, 2515 Speedway, Stop C1400, Austin, TX 78712-1205*

²*Department of Physics and Astronomy, University of North Carolina at Chapel Hill, Chapel Hill, NC 27599, USA*

³*Department of Physics, Colorado College, 14 E. Cache La Poudre St, Colorado Springs, CO 80903*

⁴*Korea Astronomy and Space Science Institute, 776 Daedeok-daero,
Yuseong-gu, Daejeon 34055, Korea*

⁵*Boston University, 725 Commonwealth Ave., Boston, MA 0215*

⁶*Physics & Astronomy Dept., Rice University, 6100 Main St., Houston, TX 77005*

(Received Jan. 1, 2018; Revised Jan. 7, 2018; Accepted November 20, 2021)

Submitted to ApJ

ABSTRACT

High-resolution, near-infrared spectra will be the primary tool for finding and characterizing Earth-like planets around low-mass stars. Yet, the properties of exoplanets can not be precisely determined without accurate and precise measurements of the host star. Spectra obtained with the Immersion GRating INfrared Spectrometer (IGRINS) simultaneously provide diagnostics for most stellar parameters, but the first step in any analysis is the determination of the effective temperature. Here we report the calibration of high-resolution H-band spectra to accurately determine effective temperature for stars between 4000-3000 K (\sim K8–M5) using absorption line depths of Fe I, OH, and Al I. The field star sample used here contains 254 K and M stars with temperatures derived using BT-Settl synthetic spectra. We use 106 stars with precise temperatures in the literature to calibrate our method with typical errors of about 140 K, and systematic uncertainties less than \sim 120 K. For the broadest applicability, we present T_{eff} -line-depth-ratio relationships, which we test on 12 members of the TW Hydrae Association and at spectral resolving powers between \sim 10,000–120,000. These ratios offer a simple but accurate measure of effective temperature in cool stars that is distance and reddening independent.

Keywords: stars: fundamental parameters, low-mass

1. INTRODUCTION

Low-mass stars ($0.1M_{\odot} < M_{*} < 0.6M_{\odot}$) represent more than 70% of the stars in the Galaxy (e.g. Reid & Gizis 1997; Bochanski et al. 2010) and approximately 40% of the stellar mass content (e.g. Mera et al. 1996; Chabrier 2005). The main-sequence lifetimes of M dwarfs, which exceed a Hubble time, makes them valuable for deciphering Galactic formation, structure, chemical evolution and dynamics. Lately, M dwarfs have become the preferred targets of exoplanet searches since, for the same size exoplanet, the transit depth and the

reflex motion produced is greater than around solar type stars (e.g. Bonfils et al. 2012; Gillon et al. 2016, 2017). Therefore, a precise determination of the stellar properties of low-mass dwarfs is fundamental to understanding astronomical questions in both the Galactic and planetary contexts.

Historically, effective temperature (T_{eff}) has been determined from photometric data (eg. Alonso et al. 1996; Masana et al. 2006; Casagrande et al. 2010; Hawkins et al. 2016), excitation equilibrium (eg. Santos et al. 2000; Sousa et al. 2011; Santos et al. 2013), line-depth ratios (eg. Gray & Johanson 1991; Biazzo et al. 2007; Fukue et al. 2015; Taniguchi et al. 2018), and spectral fitting (eg. Prugniel et al. 2011; Sharma et al. 2016; García Pérez et al. 2016). Each of these methods have

distinct applications and potential drawbacks, with the resulting temperature scales differing between them by a few-hundred Kelvin.

For example, [Veeder \(1974\)](#) and [Bessell \(1991\)](#) obtained a temperature scale for M stars by fitting a blackbody to optical and near-infrared fluxes. The [Veeder \(1974\)](#) temperature scale for stars later than M5 resulted in a much cooler sequence (~ 180 K) than that found by [Bessell \(1991\)](#). [Casagrande et al. \(2008\)](#) obtained a temperature scale for M dwarfs by modifying the infrared flux method (IFM) used for FGK dwarfs ([Casagrande et al. 2006](#)). The IFM relies on the assumption that the M star flux beyond $\sim 2.0 \mu\text{m}$ is approximately a blackbody. However, M stars have more flux than the blackbody prediction at those wavelengths ([Rajpurohit et al. 2013](#)), and as a consequence the IFM temperatures may be underestimated.

When using spectra to determine T_{eff} there is the added benefit of independent indicators for other physical properties like surface gravity and metallicity. Nevertheless, the determination of T_{eff} in low-mass stars from high-resolution infrared (IR) spectra is complicated by incomplete spectral line lists, incorrect absorption line strengths, and the presence of diatomic (e.g. TiO, FeH, OH, CO) and triatomic (e.g. H₂O) absorption bands. Despite these challenges, [Rajpurohit et al. \(2013\)](#) determined T_{eff} through a χ^2 minimization between low- and moderate-resolution ($\Delta\lambda = 10\text{\AA}$ and $\sim 4\text{\AA}$) optical ($\sim 5,200\text{--}10,000 \text{\AA}$) spectra and BT-Settl ([Allard et al. 2013](#)) synthetic spectra. Those optical spectra include atomic (Ca I, Na I, K I), diatomic (MgH, TiO, VO, CaH) and even triatomic (CaOH) absorption features. [Veyette et al. \(2017\)](#) also determined T_{eff} , [Fe/H] and [Ti/Fe] for 29 M dwarfs, but using Y-band high-resolution ($R\sim 25,000$) spectra and equivalent widths of several lines of Fe I, Ti I, and a FeH temperature-sensitive index.

More recently, [Rajpurohit et al. \(2018b\)](#) used a χ^2 minimization method and high-resolution ($R=22,000$) H-band spectra along with BT-Settl models to obtain T_{eff} , surface gravity ($\log g$) and metallicity ([Fe/H]) for 45 M dwarfs. Additionally, [Rajpurohit et al. \(2018a\)](#) used optical and near infrared ($\sim 7,500\text{--}17,000 \text{\AA}$) high-resolution ($R=90,000$) spectra to determine the stellar parameters of 292 M stars, through a χ^2 minimization against BT-Settl models for certain wavelength regions, which includes Ti I, Fe I, Ca II, Na I and OH lines. [Rajpurohit et al.](#) found a systematic offset between their determinations and those of [Passegger et al. \(2018\)](#), using the same spectra, of about 200–300 K. [Passegger et al. \(2018\)](#) used γ -TiO band, a few atomic lines (Fe I, Ti I, Ca I, Mg I) and PHOENIX-ACES ([Husser](#)

[et al. 2013](#)) models to determine T_{eff} , $\log g$ and [Fe/H]. Since both [Rajpurohit et al. \(2018a\)](#) and [Passegger et al. \(2018\)](#) used the same spectra, the discrepancy shows that T_{eff} determinations are still model-dependent. Such model-dependency can be corrected for by calibrating against empirical temperatures to obtain a calibrated temperature sequence.

Stars with physical parameters constrained by interferometric observations help to mitigate model-dependency by calibrating relationships between T_{eff} and stellar radius. For example [Mann et al. \(2013b\)](#) derived relations between temperature sensitive indexes in the visible, J, H and K bands and T_{eff} , [Newton et al. \(2015\)](#) used equivalent widths of some H-band temperature sensitive features (Mg, K, Si, CO and Al) to derive relations between T_{eff} , radius and luminosity. [Mann et al. \(2015\)](#) used spectrophotometric calibrations to derive T_{eff} , stellar radius, among other stellar parameters. The works of [Mann et al. \(2013a, 2015\)](#) and [Newton et al. \(2015\)](#) used 20+ stars with interferometric measurements to calibrate their model-independent relationships with ~ 150 K precision.

In this paper, we present the determination of T_{eff} from high-resolution ($R\sim 45,000$) H-band spectra, obtained with the Immersion GRating INfrared Spectrometer (IGRINS; [Yuk et al. 2010](#); [Park et al. 2014](#)) for 254 K and M dwarf stars. Our temperature scale is calibrated with the (r - J) color-Temperature relation from [Mann et al. \(2015\)](#). We also investigate the influence of $\log g$, projected rotational velocity ($v \sin i$), and [Fe/H] on our final results. Finally, we present T_{eff} -line-depth ratios relationships that could theoretically extend our method to any H-band spectrum with resolution $> 10,000$.

2. OBSERVATIONS AND DATA REDUCTION

This analysis makes use of spectra of K and M stars observed with IGRINS since commissioning in 2014 on the 2.7 m Harlan J. Smith Telescope (HJST) at McDonald Observatory, the 4.3 m Discovery Channel Telescope (DCT) at Lowell Observatory, and the 8.1 m Gemini South Telescope. IGRINS has no moving parts and the spectral format is fixed, with $R\sim 45,000$ over the entire H and K bands (14,500 to 24,500 \AA) ([Mace et al. 2016, 2018](#)). Changes to the input optics ensure that the spectrum is unchanged at each facility and our analysis is homogeneous.

We began with all $\sim 4,900$ IGRINS observations between 2014 July and 2018 July. Based on object name and coordinates, spectral types (SpT) and literature photometry for the entire sample were obtained from the SIMBAD database ([Wenger et al. 2000](#)) in Jan-

uary 2019. The large list of references and methodologies used to assign the spectral types listed in SIMBAD result in spectral type uncertainties of ± 1 -2 subtypes. Spectral types were used in our analysis to provide an initial estimate of T_{eff} and guide the search for atomic/molecular lines sensitive to changes in T_{eff} and then to provide a T_{eff} -SpT relation. Giant and young stars were removed from further consideration through photometric selection using M_K magnitudes derived from 2MASS photometry and Gaia DR2 parallaxes. We find that giants have $M_K < 0$, and YSOs are more than 1 magnitude brighter than the field M dwarf trend identified by Mann et al. (2015). Such selection criteria did not rid our sample of binary stars, especially in cases where the component masses and fluxes differ significantly, and there is a possibility that our sample includes single- and double-lined spectroscopic binaries. The final sample we consider contains 254 stars (41 K, 198 M and 15 unknown spectral types) with 2MASS H-band magnitudes from 3 to 12. Many of the 254 stars in this sample are well known field stars included in the analyses of Mann et al. (2015); Rojas-Ayala et al. (2012); Newton et al. (2015); Mann et al. (2018) and presented previously in the IGRINS Spectral Library (Park et al. 2018)¹.

We observed each star in our sample by nodding between two positions on the slit to facilitate the removal of sky background and telluric emission lines in data reduction. Single frame exposure times range from 30 to 900 s with the goal of achieving $\text{SNR} \gtrsim 100$ per resolution element for each observation, however, 85 objects in our sample have SNR less than 100 due to conditions at the time of the observations and/or the faintness of the star. The average SNR for the sample is ~ 160 . A0V standard stars were observed at a similar airmass before or after each science object and used for telluric correction.

All the spectroscopic data were reduced using the IGRINS pipeline (Lee, Gullikson, & Kaplan 2017)², which performs flat-field correction, wavelength calibration using night sky OH emission and telluric absorption lines, A-B frame subtraction to remove skyline emission, and the extraction of the one-dimensional spectrum following the optimal methods of Horne (1986). Telluric absorption lines were corrected by dividing the science spectrum by the A0V spectrum, which had been multiplied by the Vega model of Kurucz (1979). A representative sample of the IGRINS spectra in our sample is shown in Figure 1.

¹ http://starformation.khu.ac.kr/IGRINS_spectral_library

² <https://github.com/igrins/plp/tree/v2.1-alpha.3>

3. SPECTRAL ANALYSIS

Stellar spectra are primarily shaped by T_{eff} , $\log g$ and $[\text{Fe}/\text{H}]$. When deriving these parameters using high-resolution spectra, stellar activity, $v \sin i$ and magnetic field strength (B) should also be considered.

To identify temperature sensitive spectral regions in the IGRINS spectra we first sorted the spectra by the literature spectral types. We estimated the radial velocity of each star by finding the wavelengths offset of the Na I doublet at ~ 22056 and 22084 \AA , and then we shifted all spectra to the same rest-frame wavelength. This process assumed that all the stars in the sample have roughly the same $\log g$ and $[\text{Fe}/\text{H}]$. Through visual inspection we identified some new regions with T_{eff} sensitivity and spectral regions that have been previously used by similar studies (eg. Prato et al. 2002; García Pérez et al. 2016; Rajpurohit et al. 2018b). We ultimately selected strong absorption lines that were close enough to each other to reside in the same IGRINS spectral order and that displayed opposite line strength variation versus SpT (T_{eff}) (i.e. one line grew weaker and the other grew stronger when looking at progressively later spectral types). Finally, we repeated the visual inspection using synthetic spectra and selected lines with low sensitivity to changes in $\log g$ or $[\text{Fe}/\text{H}]$. From our visual inspection process we identified two spectral regions, bounding OH (15600 – 15650 \AA) and Aluminum (16700 – 16780 \AA) absorption features, that reliably trace T_{eff} .

The determination of $v \sin i$ for the IGRINS spectra relied on the code developed by Kesseli et al. (2018). In spectral type bins of K0-K3, K4-K6, K7-K9, M0-M1, M2-M3, M4-M5, M6-M9 we identified template objects by their narrow lines and high signal-to-noise ratios. We selected HD 88925, HD 122120, GJ 169, GJ 15A, GJ 725A, GJ 15B, GJ 412B as our template stars for each of the spectral type bins listed above, respectively. We were able to determine $v \sin i$'s spanning between 7 and 53 km s^{-1} for 156 stars of our sample, with $\sim 56\%$ between 7 and 12 km s^{-1} . The remaining stars have $v \sin i$ below the IGRINS spectral resolution and were assigned $v \sin i = 7 \text{ km s}^{-1}$.

3.1. Synthetic spectra

Once the OH and Al regions were identified as the best T_{eff} indicators in the IGRINS spectra of K and M stars, we looked for a theoretical counterpart (synthetic spectra) suitable for assigning temperatures. The BT-Settl models (Allard et al. 2013; Baraffe et al. 2015) have previously been validated in the range $2500 \leq T_{\text{eff}} \leq 4000 \text{ K}$ at low ($\Delta\lambda = 10 \text{ \AA}$; e.g. Rajpurohit et al. 2013) and high ($R = 22,000$ and $90,000$; e.g. Rajpurohit et al. 2018b,a)

spectral resolution, and is the preferred set of synthetic spectra for our study. We employed the CIFIST³ version, which cover the parameter space $T_{\text{eff}} = 300 - 7000$ K, $\log g = 2.5 - 5.5$, $[\text{Fe}/\text{H}] = -2.5 - 0.0$ at high-resolution ($R \sim 330,000$ at 16500 \AA). These set of spectra were computed with the PHOENIX code (Hauschildt et al. 1997), the Caffau et al. (2011) solar abundances and an updated atomic and molecular line opacities (see Baraffe et al. 2015, and references therein), which dominate the optical and near-infrared spectra of cool stars.

The synthetic spectra (or model) grid used in this work spans T_{eff} between 2000 and 4700 K in steps of 100 K, $\log g = 4.0, 4.5$, and 5.0 , solar metallicity and no alpha-element enrichment. The resolution of the synthetic spectra were degraded to the IGRINS spectral resolution ($\sim 45,000$). For all temperature determinations, we selected models with $\log g$ of 4.5 since it is suitable for both K (e.g. $\log g \sim 4.4 \pm 0.1$; Sousa et al. 2008; Tsantaki et al. 2013) and M (e.g. $\log g \sim 4.8 \pm 0.2$; Ségransan et al. 2003; Berger et al. 2006) field stars. The remaining models with $\log g$ of 4.0 and 5.0 were employed just to assess the impact of $\log g$ on our analysis. The grid of synthetic spectra was broadened to the rotation velocities encompassing the IGRINS sample $v \sin i$'s (7 to 55 km s^{-1}) using the function `rotBroad`, available in the PyAstronomy library⁴. The rotational broadening kernel requires a linear limb-darkening coefficient, which we estimated by comparing the model T_{eff} and $\log g$ to Claret et al. (2012)⁵ catalog. Finally, vacuum wavelengths provided with BT-Settl spectra were converted to their corresponding air wavelengths following the IAU standard formulation (Morton 1991).

In summary, the grid of synthetic spectra used for measuring line-depths in the OH and Al regions had $T_{\text{eff}} = 2000 - 4700$ K, $\log g = 4.5$, $[\text{Fe}/\text{H}] = 0.0$, $v \sin i = 7 - 55 \text{ km s}^{-1}$, spectral resolution of $45,000$ and no α -element enrichment. Figure 2 shows how the line-depth behavior in the IGRINS spectra is well reproduced by the BT-Settl models, including the flux peak in the Al region (right panel of Figure 3).

3.2. OH region (15600 – 15650 Å)

The OH region spans 15600 to 15650 \AA and includes two Fe I lines ($\lambda \sim 15621.6$ and 15631.9 \AA) and an OH

($\lambda_{\text{OH}} \sim 15627.0 \text{ \AA}$) doublet. These lines change as a function of spectral type (Prato et al. 2002) as can be seen in the left panel of Figure 1. The Fe I line that we used here ($\lambda_{\text{Fe}} = 15621.6 \text{ \AA}$) becomes weaker at lower temperatures and is un-blended in the temperature region we are interested in. The OH feature, which is formed by two OH lines at approximately 15626.7 \AA and 15627.5 \AA , increases in depth at lower temperatures, up to $\sim \text{M4-M5}$ stars, where numerous H_2O features start to dominate the spectral region.

3.3. Al region (16700 – 16780 Å)

The Al region covers 16700 to 16780 \AA , and contains three different Al lines ($\lambda \sim 16719.0, 16750.6$ and 16763.4 \AA). The strongest Al I line is at $\lambda_{\text{Al}} = 16750.6 \text{ \AA}$ and is present in objects with spectral types between approximately K3 and M6-7. The line depth of Al I remains unchanged for the late-type K and early-type M stars, but then decreases at lower temperatures. The second feature, which is located around $\lambda_{\text{peak}} = 16745.9 \text{ \AA}$ is a flux bump that rises at lower temperatures. The peak flux is the result of an atmospheric transmission window (the absence of absorbers) in the star, and is coincident with the disappearance of Fe in the OH region. This flux peak is sensitive to T_{eff} beginning in M4 stars and later. The contrary dependence of the Al and peak flux line depths to T_{eff} is as useful as deriving T_{eff} as the OH and Fe line depths, but at lower temperatures.

3.4. Determining T_{eff}

At the IGRINS spectral resolution the Fe line that we used is un-blended, the OH lines are blended but approximately equal in depth, the flux peak is created by the absence of absorption within the broad absorption defining the pseudo-continuum, and the broad Al line is blended with OH and CO at high and low temperatures, respectively. These characteristics of the lines make equivalent width measurements inconsistent across a broad sampling of spectral types. Yet, we find that line-depths consistently trace T_{eff} (see Figure 3) and here we describe our methods.

3.4.1. Line-depth Measurements

As mentioned before, molecular lines dominate the atmospheres of cool stars and complicate the determination of a continuum level, which leads to inconsistencies in spectral normalization. To address this issue, we computed the median flux across the entire OH or Al region and used this value to normalize our spectra within those regions. Continuum fitting using the average flux across the region, or a smoothed spectrum, did not produce

³ <https://phoenix.ens-lyon.fr/Grids/BT-Settl/CIFIST2011-2015/>

⁴ <https://github.com/sczesla/PyAstronomy>

⁵ We used the filter H (2MASS) linear limb-darkening coefficients. For those T_{eff} and $\log g$ values that were not reported in Claret et al. (2012), we have used the nearest (in terms of T_{eff} and $\log g$) coefficient available, in those cases where there were more than one possible coefficient we assigned an average.

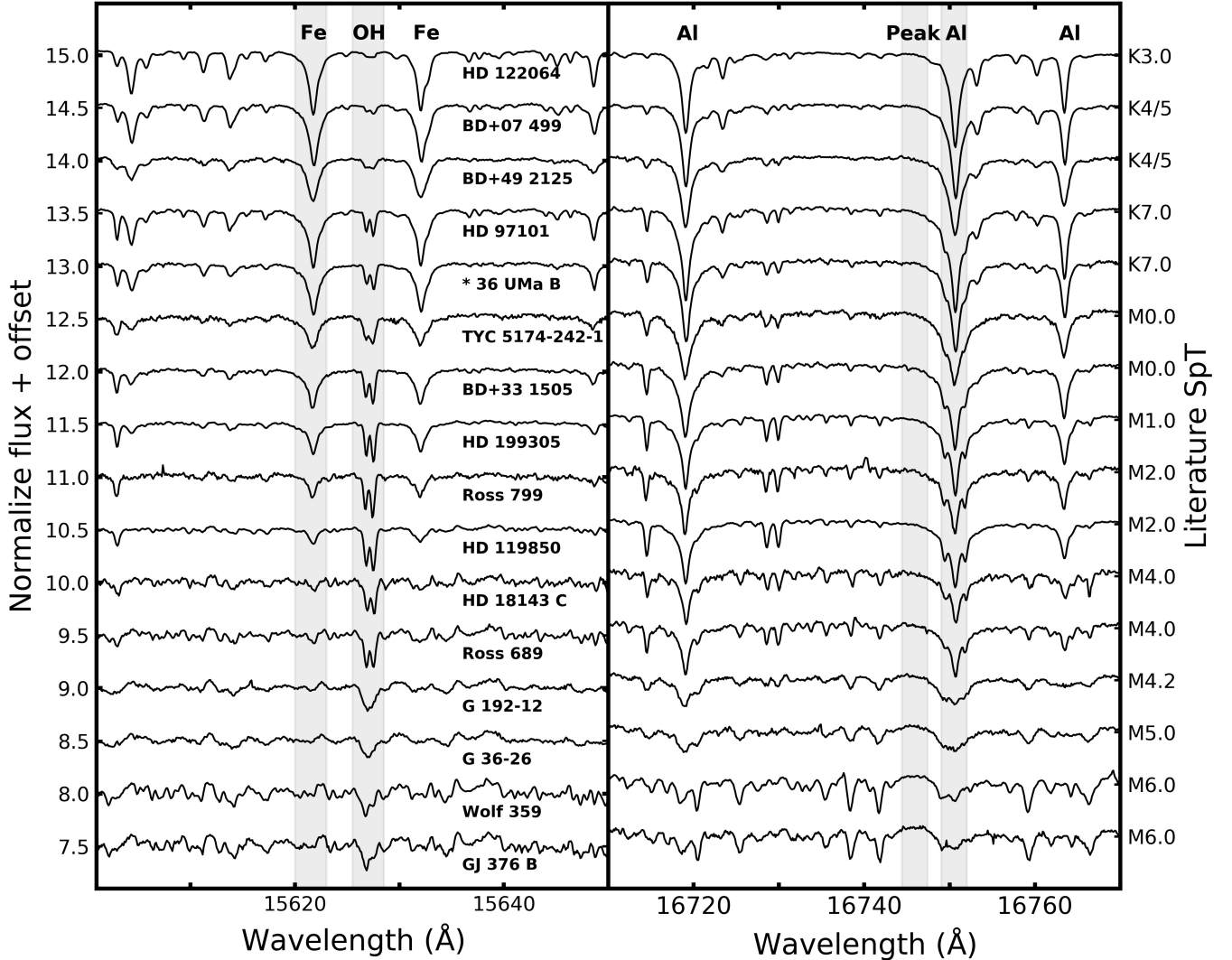


Figure 1. A representative sample of IGRINS K and M star spectra around the OH region and the central 60 Å of the Al region, as a function of spectral type. The spectral lines used in this work are highlighted in gray, while other prominent lines are also labeled. The dependency of the selected lines with SpT (T_{eff}) is clearly present. The Al region is effective for stars later than \sim M4 while the OH region is effective for stars earlier than \sim M4.

a consistent definition of the continuum for all spectra. More complicated determinations of the continuum using iterative sigma clipping, or the upper quartile of the flux within the region, produces the same results as using the median but with some constant offset. The spectra in Figure 2 have been normalized by the median flux, and while this may not provide the most accurate determination of the continuum level, it produces repeatable measurements when applied uniformly across the entire analysis. Since we normalize the BT-Settl models in the same fashion, and these models accurately reproduce the spectra of our stars, any inaccuracy in the normalization is consistently applied to all spectra.

After normalizing the spectrum, we searched within ± 1.5 Å of the the central wavelengths (λ_{OH} , λ_{Fe} , λ_{Al} ,

λ_{peak}) for the minimum flux value of the Fe I, OH, Al I lines and the maximum for the flux peak. We then computed the average flux (\bar{f}_{λ}) and the standard deviation of the mean (σ_f) within a window of 5 pixels (~ 1.5 resolution elements), centered at the min/max found previously. The measured line depth (flux peak height) is $d = 1 - \bar{f}_{\lambda}$ and we assign σ_f as the uncertainty. The line depths were determined the same way in the observed and synthetic spectra. The line depths from the synthetic spectra defined a matrix of values for each spectral region, where the corresponding depths are identified by the unique T_{eff} and $v \sin i$ combination of the model grid.

In Figure 3 we present the synthetic line-depths as a function of T_{eff} and $\log g$. Adding the dependence to $\log g$ in this figure help us to examine, in a qualitative

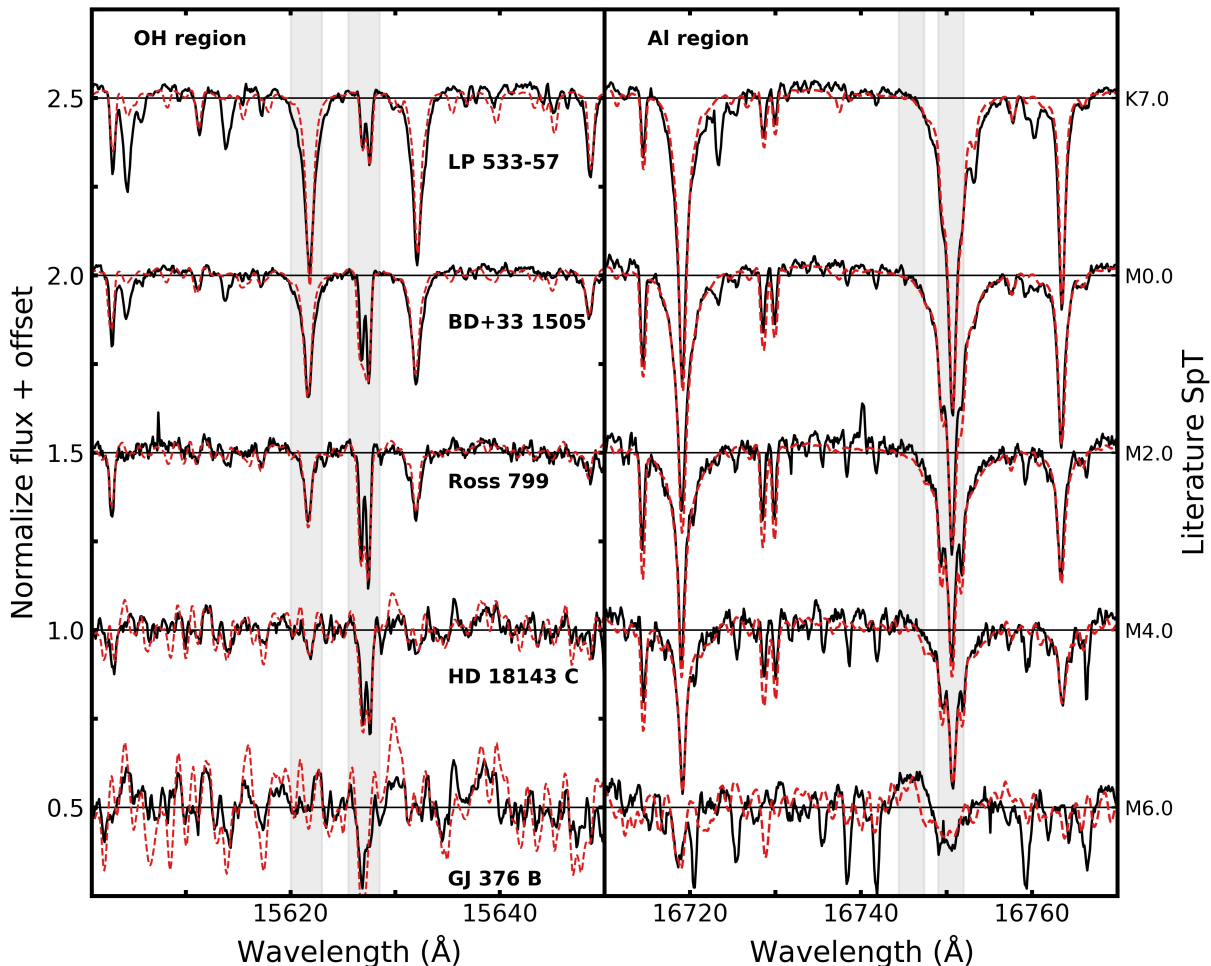


Figure 2. A representative sample of IGRINS (black solid line) and synthetic BT-Settl (red dashed line) spectra around the OH region and the central 60 Å of the Al region as a function of spectral classification. The horizontal lines represent the median flux across the region of interest and the level where line-depths are measured. These regions also include several other atomic (Fe I, Ti I and Ni I) and molecular (FeH, CN and CO) lines that are not labeled here and absent in the synthetic spectra.

way, how our T_{eff} determination is modulated by variations in $\log g$. In the synthetic spectra, the Fe I line depth increases monotonically for $T_{\text{eff}} > 3000$ K (SpT earlier than $\sim M5$) and it appears to saturate around 4500 K ($\sim K4$). By contrast, the OH depth increases more slowly to a maximum value at ~ 3600 K ($\sim M2$) and then decreases up to ~ 4700 K ($\sim K3$).

The synthetic line depth of the flux peak, which by our definition is negative since it is above the pseudo-continuum, increases monotonically from 2300 K ($\sim M9$) to ~ 3200 K ($\sim M4$). The Al I line depth decreases linearly with decreasing T_{eff} . The role of $\log g$ in the Al region seems less important than in the OH region, since the changes on T_{eff} produced by ± 0.5 in $\log g$ are ~ 120 K and ~ 90 K for the flux peak and the Al I line. Additionally, increasing gravity reduces both the amplitude of the peak flux and the line depth of the Al line.

Another advantageous feature of these spectral regions is the range of SpT over which they are sensitive to T_{eff} . Together, they allow us to determine the T_{eff} scale for $\sim K8$ to M5 stars. While the Al region is appropriate for late-type objects ($\sim M4$ and later) the OH region is useful for SpTs earlier than $\sim M5$, having an overlapping zone of about 1 sub-class in SpT.

In the analysis that we present here we assume that $\log g = 4.5$ for all the targets in our sample and we adopted solar metallicity. These assumptions were made because our targets are nearby field stars that most probably reside in the thin disk (eg. [Reylé et al. 2002](#)). We investigate the impact of these assumptions on our final determination of T_{eff} in Sections 4.1.1 and 4.1.2.

3.4.2. A Precise T_{eff} Sequence

For each pair of line-depths we performed a χ^2 minimization between the observed star and the synthetic

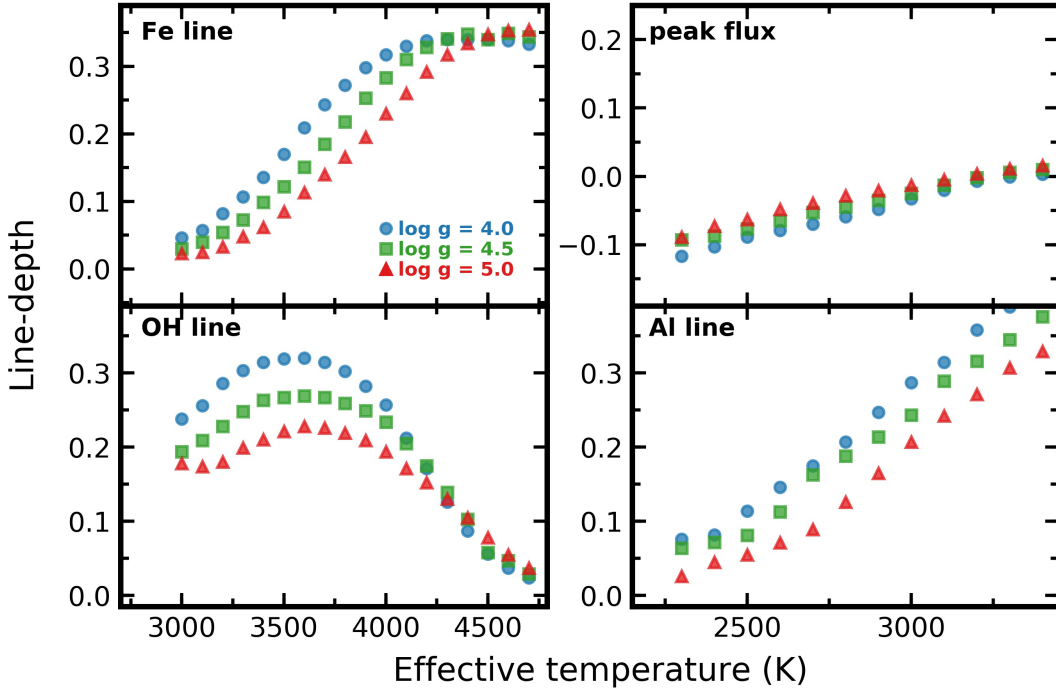


Figure 3. BT-Settl synthetic line depths as a function of effective temperature, color-coded by surface gravity. The synthetic line-depths of both regions exhibit a strong contrary dependence to T_{eff} and a weaker one to $\log g$.

line-depth grid corresponding to the star’s $v \sin i$. The derived line-depth temperature (T_{LD}) was taken as the weighted mean of the temperatures corresponding to the minimum and the two closest χ^2 values. The uncertainty in the temperature determination ($\sigma_{T_{\text{LD}}}$) was measured as:

$$\sigma_{T_{\text{LD}}} = \frac{n}{(n-1)W^2} \sum_i w^2 (T_i - T_{\text{LD}})^2 \quad (1)$$

where $n(=3)$ is the number of measurements used in the weighted average, $W = \sum_i w$, w is the weight ($= 1/\chi^2$), T_i is the model temperature and T_{LD} is the weighted mean temperature. When the minimum χ^2 corresponded to the lower or upper edges of the synthetic line-depth grid then the derived temperature was given a null value.

From the measured line depths of the K and M stars in our sample we assigned T_{eff} to each star based on the line depths of the synthetic spectra. T_{eff} was determined by means of the OH region in 116 stars, the Al region in 92 stars, and using both spectral regions for 46 stars.

While the IGRINS spectra were well matched by the BT-Settl models (Figure 2), the temperature scale obtained using theoretical grids are generally precise, but also inaccurate. The inaccuracy stems from the different physical assumptions of the stellar structure, atomic and molecular line lists, and the modeler’s treatment of the line strengths.

In the following section we used the empirical color-Temperature relation of Mann et al. (2015) to take into account discrepancies in the temperature scale between models and observation.

3.4.3. Accurate T_{eff} ’s for K and M Stars

Mann et al. (2015) used accurate spectrophotometric calibrations to determine T_{eff} , bolometric flux, metallicity, and stellar radii for 183 nearby K7 – M7 stars. Those T_{eff} values were calibrated by means of temperatures determined from interferometric data for 29 stars, resulting in an empirical temperature scale.

Interferometrically determined temperatures are accurate for the range of stellar parameters that are covered by the sample itself. For the 51 stars we have in common with the Mann et al. sample, only 14 of these have interferometric data. We chose to calibrate our line-depth temperatures from the models above to empirical scale, by means of their (r - J) color-Temperature relation, instead of using the stars in common. The (r - J) color-Temperature relation determined by Mann et al. (2015) is tied to the interferometric stars and is valid for $2700 < T_{\text{eff}} < 4100$ K:

$$T_{\text{emp}} = 3500 \times (a + bX + cX^2 + dX^3 + eX^4) \quad (2)$$

where a , b , c , d , and e are the polynomial coefficients found by Mann et al. (2015), with values of 2.84, -

1.3453, 0.3906, -0.0546 and 0.002913, respectively, and X is the (r - J) color in magnitudes. We retrieved the available r- and J-band photometry for all our sample from the AAVSO All-Sky Photometric Survey (APASS; Henden et al. 2012) and the Two Micron All Sky Survey (2MASS; Cutri et al. 2003), and then computed empirical temperatures using the above equation. The photometric data and the (r - J) color temperatures are reported in Table 1. The calibration sample comprises 106 stars in the Mann et al. sample and the IGRINS sample, from which 66 were determined with the AI region and 64 from the OH region (24 stars are in both regions).

Figure 4 illustrates how the derived temperatures from both spectral regions correlate linearly with the (r - J) color temperatures. The temperatures determined using the AI region primarily exhibit an offset of ~ 640 K with respect to the empirical temperatures, while those determined using the OH region display a steeper slope with respect to their empirical counterparts. The equations in Figure 4 were used to convert the precise line-depth temperature sequence into an accurate one calibrated against the Mann et al. sample. These empirically calibrated temperatures (T_{spec}) are considered the final measurements. We assigned for the stars with temperatures determined in both the OH and AI regions an average of their corresponding calibrated temperatures, and the sum in quadrature of the individual errors is the final uncertainty.

4. RESULTS AND DISCUSSION

In Table 1 we report the temperatures we derive along with basic information for all 254 K and M field stars. Although the compiled SpT of our sample is precise to only ± 1 -2 subtypes, we constructed a SpT- T_{spec} relation (see Figure 5 and Table 2) to compare with temperature scales determined for dwarf stars by Pecaut & Mamajek (2013) and the median results of Rajpurohit et al. (2013). Both studies used BT-Settl models, but with the solar composition of Asplund et al. (2009) and Caffau et al. (2011), respectively. Pecaut & Mamajek (2013) determined T_{eff} by using the Spectral Energy Distribution Fitting method (SEDF; Masana et al. 2006), which simultaneously fits the observed and synthetic photometry. On the other hand, Rajpurohit et al. (2013) compared low- and medium-resolution ($\Delta\lambda = 10$ and 4 \AA) optical spectra with BT-Settl models to determine temperature.

We found good agreement between Rajpurohit et al. (2013), Pecaut & Mamajek (2013) and this work for objects with SpT between K6-M6, where the maximum difference with our median temperatures is 150 K, being

of the order of our typical error ($\sigma_{\text{typ}} = 140$ K). In the cases of the K5 and M7 bins these differences increased up to 245 K ($\sim 1.8\sigma_{\text{typ}}$). A fourth degree polynomial fit to the median temperature per SpT bin provides the equation:

$$T_{\text{spec}} = a + bX + cX^2 + dX^3 + eX^4 \quad (3)$$

where X is the SpT and takes numerical values between 4 and 17 (equivalent to SpT K4 to M7) and $a, b, c, d,$ and e are the fitted polynomial coefficients equal to 3973.570, 74.705, -4.140, -0.821, 0.034, respectively.

4.1. Sources of uncertainty in T_{spec} measurements

Besides the literature SpT, another possible source of scatter in Figure 5 could be the fixed values we chose for $\log g$ and $[\text{Fe}/\text{H}]$. Although these are reasonable assumptions for our sample of field dwarfs, in the next sections we investigate the potential impact of these two parameters on the T_{eff} scale.

4.1.1. Metallicity effects

Along with T_{eff} , Mann et al. (2015) also reported metallicities determined from equivalent widths of atomic features in low-resolution near-infrared spectra. Such metallicities were calibrated by means of wide binary systems with FGK primary stars and M dwarf companions (Mann et al. 2013a, 2014).

For the 51 stars in common with Mann et al. (2015), we explore trends related to $[\text{Fe}/\text{H}]$. Although this comparison is not independent, since we corrected our temperatures with the Mann et al. (2015) color-Temperature relation, it is still meaningful to better understand the role of $[\text{Fe}/\text{H}]$ on the derived temperature scale.

The left panel of Figure 6 depicts the comparison between T_{spec} and the Mann et al. temperatures, color-coded by the metallicities of Mann et al. The $[\text{Fe}/\text{H}]$ of the stars in common with Mann et al. (2015) spans from -0.38 to +0.39 dex, which we have classified into three categories: metal-poor ($[\text{Fe}/\text{H}] < -0.10$), solar composition ($-0.10 \leq [\text{Fe}/\text{H}] \leq +0.10$) and metal-rich ($[\text{Fe}/\text{H}] > +0.10$) stars. Using these metallicity classifications we identified 20 metal-poor, 18 solar composition and 13 metal-rich stars. We computed the reduced chi-square (χ^2_{ν}) between our observations and the literature values as a measurement of the agreement between the two temperatures. We found χ^2_{ν} value of 1.2, 0.8 and 1.2 for the metal-poor, solar composition and metal-rich stars.

The good agreement with the solar composition stars is not surprising since we derived T_{eff} from solar metallicity models. We expected some temperature variations

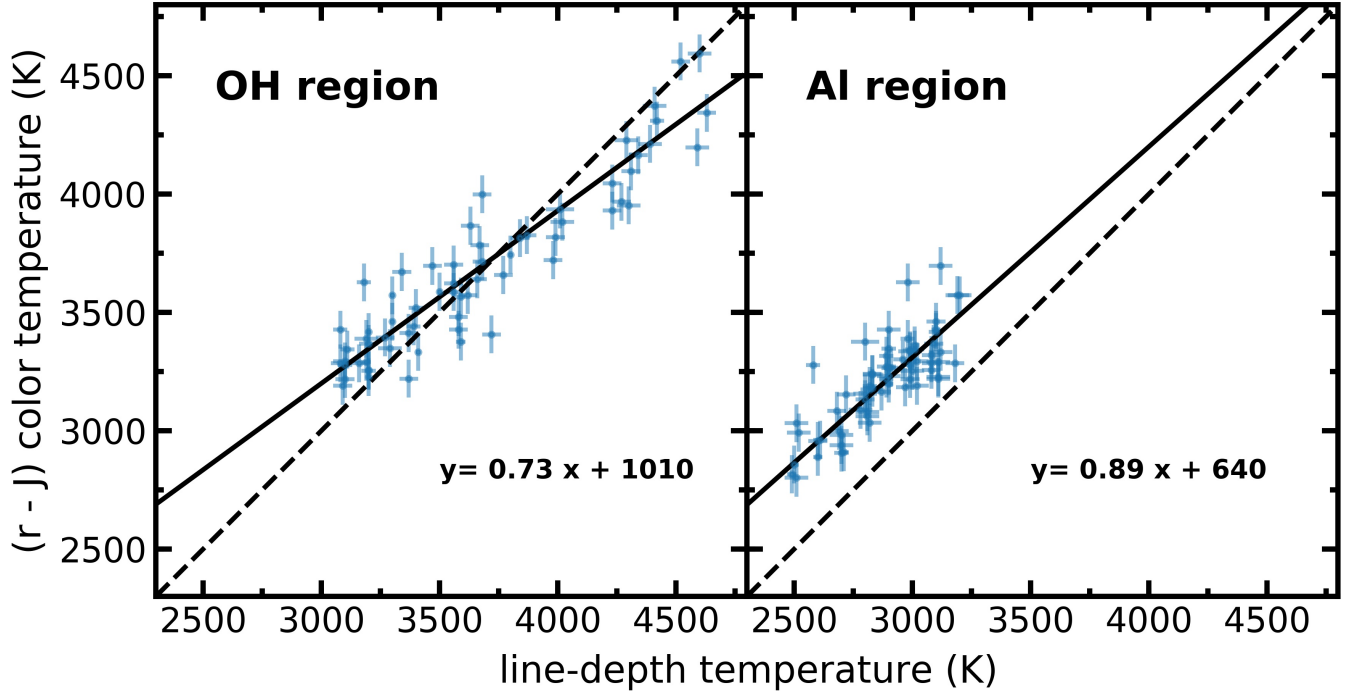


Figure 4. Comparison between the T_{eff} determined in this work through Al and OH region and their corresponding empirical temperatures. The dashed line represents the one-to-one relation while the solid one is the weighted linear fit. Errors on empirical temperatures are all assumed to be 80 K, which is the quadrature sum of the typical spectroscopic error (60 K) and the dispersion of the calibration (58 K) as reported in Mann et al. (2015).

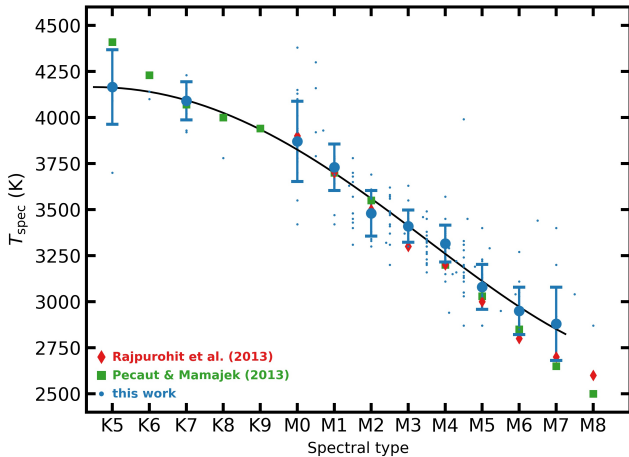


Figure 5. Our T_{spec} (small circles) as a function of the literature SpT. The solid line is a weighted fourth degree polynomial fit to the median values of T_{spec} (large circles) to non-fractional SpT with more than two stars, while the error bars represent the one standard deviation level. The squares are the temperature scale for dwarfs stars of Pecaut & Mamajek (2013) and the diamonds are the results of Rajpurohit et al. (2013).

as the stellar metallicity departs from the solar value because the line-depths appear deeper/shallower as $[\text{Fe}/\text{H}]$ increases/decreases.

Rojas-Ayala et al. (2012) also estimated T_{eff} and $[\text{Fe}/\text{H}]$, but using equivalent widths of the Ca ($\sim 22,050 \text{ \AA}$) and Na ($\sim 22,630 \text{ \AA}$) lines, as well as the $\text{H}_2\text{O-K2}$ index, in low-resolution ($R \sim 2,700$) K-band spectra. We have in common with Rojas-Ayala et al. (2012) 47 stars that we compare in the middle panel of Figure 6. The overall χ^2_ν of this comparison is 1.7 and we found a slight trend, which highlights a systematic difference between our methods since T_{eff} smaller (larger) than $\sim 3300 \text{ K}$ seems to be underestimated (overestimated). Such a trend was also pointed out by Mann et al. (2015). We found $\chi^2_\nu = 2.0$ for 18 metal-poor, $\chi^2_\nu = 2.2$ for 18 solar composition and $\chi^2_\nu = 0.7$ for 11 metal-rich stars. The cause of the trend in ΔT_{eff} compared to Rojas-Ayala et al. (2012) is likely because they used an older version of the BT-Settl models, which employs the solar abundances of Asplund et al. (2009) rather than the Caffau et al. (2011) and an older versions of line lists.

Finally, in the right panel of Figure 6, we compared our determinations with those made by Rajpurohit et al. (2018a), which determined T_{eff} , $\log g$ and $[\text{Fe}/\text{H}]$ from optical and near infrared ($\sim 7,500\text{--}17,000 \text{ \AA}$) high-resolution ($R=90,000$) spectra. The general comparison resulted in $\chi^2_\nu = 1.7$, while the comparison by category is $\chi^2_\nu = 2.0$, $\chi^2_\nu = 1.1$, and $\chi^2_\nu = 1.9$, for 14 metal-poor, 11 solar composition, and 16 metal-rich

Table 1. Basic information as well as our results for the first 20 entries of our sample. We compile SpT, r and J magnitudes, the empirical temperatures ($T(r-J)$), rotational velocity, the four line-depths, an identification number corresponding to the source of the temperature being, 1 from OH region, 2 from Al region, 3 from the average of both regions and 4 if it is a limit, and in the final column we report our T_{spec} . The full version of this table will be available in the online version of the paper.

Star	SpT	Ref. ^a	J	r	T(r-J)	$v \sin i$	normalize flux line-depths				reg	T_{spec}^b
							Fe I	OH	peak	Al I		
			(mag)	(mag)	(K)	(km s^{-1})					(K)	
LP 699-32	0	1	10.67	15.59	2889	10	–	–	-0.075 ± 0.006	0.127 ± 0.006	2	2950 ± 110
NLTT 55442	0	1	10.39	15.04	2962	18	–	–	-0.069 ± 0.004	0.121 ± 0.004	2	2960 ± 110
LSPM J2206+4322W	0	1	10.78	–	–	–	0.058 ± 0.002	0.190 ± 0.020	-0.044 ± 0.005	0.320 ± 0.010	3	3360 ± 90
G 194-18	0	1	10.56	13.74	3427	<7	0.041 ± 0.003	0.200 ± 0.100	-0.031 ± 0.004	0.308 ± 0.006	3	3330 ± 90
G 122-46	0	1	10.59	–	–	8	0.040 ± 0.010	0.250 ± 0.020	–	–	1	3270 ± 140
NLTT 19346	0	1	11.76	–	–	–	–	–	-0.073 ± 0.004	0.116 ± 0.003	2	2950 ± 110
UCAC4 368-064862	0	1	9.27	11.81	3702	<7	0.160 ± 0.007	0.240 ± 0.020	–	–	1	3610 ± 140
[RSP2011] 315	0	1	11.01	14.23	3413	–	0.110 ± 0.010	0.220 ± 0.020	–	–	1	3470 ± 140
UCAC4 445-057351	0	1	9.76	13.25	3320	12	–	–	-0.042 ± 0.003	0.265 ± 0.003	2	3380 ± 120
LP 611-70	0	1	9.51	–	–	9	0.235 ± 0.009	0.210 ± 0.030	–	–	1	3790 ± 130
G 43-43	0	1	9.41	12.11	3623	<7	0.160 ± 0.004	0.240 ± 0.020	–	–	1	3610 ± 140
UCAC4 545-148763	0	1	9.17	11.50	3826	8	0.255 ± 0.006	0.200 ± 0.020	–	–	1	3840 ± 140
2MASS J12371238-4021480	0	1	9.47	12.88	3347	–	–	–	-0.033 ± 0.001	0.218 ± 0.002	2	3220 ± 110
2MASS J04435750+3723031	0	1	12.22	–	–	–	–	–	-0.083 ± 0.004	0.113 ± 0.003	2	2950 ± 110
BD+45 598	K0.0	2	7.62	8.80	–	19	0.247 ± 0.004	0.000 ± 0.002	–	–	4	4440 ± 130
HD 285690	K0.0	2	7.88	9.24	–	10	0.400 ± 0.010	0.008 ± 0.003	–	–	4	4440 ± 130
HD 286363	K0.0	3	8.18	9.72	–	11	0.400 ± 0.010	0.025 ± 0.003	–	–	4	4440 ± 130
HD 285482	K0.0	3	8.11	9.56	–	11	0.400 ± 0.010	0.016 ± 0.001	–	–	4	4440 ± 130
HD 285876	K0.0	4	8.67	10.51	4212	11	0.380 ± 0.010	0.110 ± 0.010	–	–	1	4210 ± 140

^a Reference for SpT shown in SIMBAD at the time of the query (March 2019).

^b The error reported is just the random uncertainties, while the systematic ones were estimate in Section 4.1.4 and are of ± 120 K.

References—(1)No specified; (2)Cenarro et al. (2007); (3)Nesterov et al. (1995); (4)Benedict et al. (2014) (5)Keenan & McNeil (1989); (6)Houk & Cowley (1975); (7)Houk & Swift (1999); (8)White et al. (2007); (9)Stephenson (1986a); (10)Stephenson (1986b); (11)Bidelman (1985); (12)Reid et al. (2004); (13)Koen et al. (2010); (14)Fekel & Bopp (1993); (15)Torres et al. (2006); (16)Alonso-Floriano et al. (2015); (17)Gray et al. (2003); (18)Henry et al. (2002); (19)Schlieder et al. (2012b); (20)Kirkpatrick et al. (1991); (21)Lépine et al. (2013); (22)Riaz et al. (2006); (23)Shkolnik et al. (2009); (24)Bouy & Martín (2009); (25)Schlieder et al. (2012a); (26)Mann et al. (2013a); (27)Kraus et al. (2014); (28)Joy & Abt (1974); (29)Newton et al. (2014); (30)Pesch & Bidelman (1997); (31)von Braun et al. (2014); (32)Terrien et al. (2015); (33)Davison et al. (2015); (34)Reid et al. (2007); (35)Walker (1983); (36)Gomes et al. (2013); (37)Aberasturi et al. (2014); (38)Rojas-Ayala et al. (2012); (39)Reid & Walkowicz (2006); (40)Law et al. (2008); (41)Mann et al. (2016); (42)Herczeg & Hillenbrand (2014); (43)Montagnier et al. (2006); (44)Mann et al. (2014); (45)Scholz et al. (2005); (46)Bowler et al. (2015); (47)Gagné et al. (2015); (48)West et al. (2015); (49)Gigoyan & Micaelian (2012); (50)Schmidt et al. (2007).

stars, respectively. There is not an obvious trend with metallicity, but the comparison shows a larger dispersion than our comparison to Mann et al. (2015).

The result of these three comparisons reveals that our temperature scale is consistent with previous ones, giving us the ability to determine accurate T_{eff} for any star within the IGRINS archive without the necessity of extra data, such as photometry. Additionally, we found that a difference in metallicity of $\Delta[\text{Fe}/\text{H}] = \pm 0.4$ will have the effect of change our temperatures by $\Delta T_{\text{spec}} = \mp 100$ K. In other words, our method will produce hotter and cooler temperatures for metal-rich and metal-poor stars, respectively.

Another important point comparison between this work and previous works is the value of $\log g$. Since we calibrated our temperatures with the relationship from Mann et al. (2015), the impact of using different $\log g$ values was taken into account, as the good agreement ($\chi^2_{\nu} = 1.0$) showed. However, the differences found with Rojas-Ayala et al. (2012) and Rajpurohit et al. (2018a) could be caused by $\log g$ differences since they measured $\log g$ rather than making it a fixed quantity.

4.1.2. Surface gravity effects

To characterize the effects of surface gravity on our temperature sequence we chose synthetic models with $\log g = 4.0$ and 5.0 and determined T_{eff} following the same line-depth method outlined in Section 3.4. With this approach we treat the synthetic spectra as a star with a known $\log g$ value that we determine its temperature for with the $\log g = 4.5$ models.

In Figure 7 we show the results obtained in this test. We found that $\log g$ is not important for $T_{\text{eff}} \gtrsim 4100$ K, an advantage of the OH region seen also in Figure 3. For the synthetic spectra with $\log g = 4.0$ and T_{eff} between 3100 and 3900 K, we find hotter temperatures of ~ 140 K on average. For the synthetic spectra with $\log g = 5.0$ our method recovered temperatures on average ~ 160 K cooler. Below ~ 3100 K the behavior is slightly different for $\log g = 4.0$, in that the temperatures cross the one-to-one line, while for spectra with $\log g = 5.0$ are consistently cooler.

Averaging the mean differences found in the different temperature ranges we establish that a change in $\log g$ of 0.5, will modify our T_{eff} by ~ 150 K. This effect will result in hotter temperatures for stars with $\log g$ lower

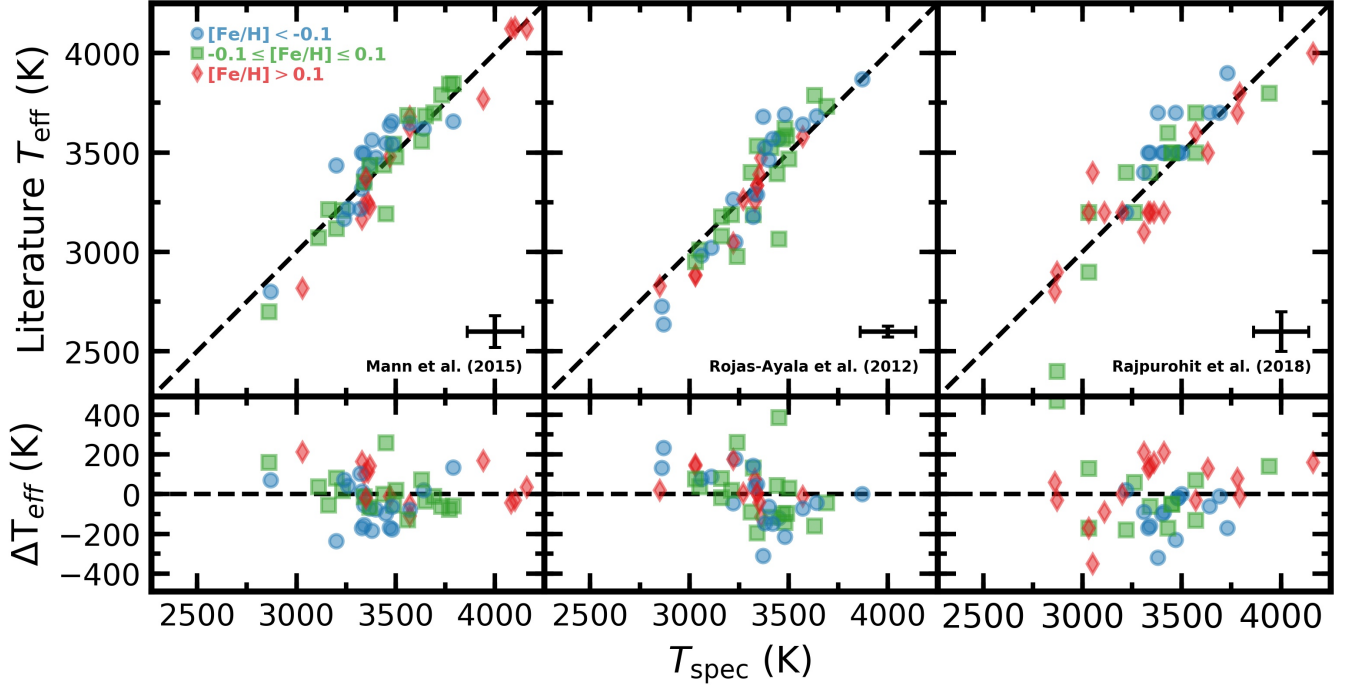


Figure 6. Comparison between our T_{spec} (x-axis) and those determined by Mann et al. (2015) (left), Rojas-Ayala et al. (2012) (middle) and Rajpurohit et al. (2013) (right), color-coded by their metallicity determinations. The lower panels show the residuals of our derived T_{eff} minus the literature temperatures. The mean error in each panel is about 80, 30 and 100 K, for Mann et al. (2015), Rojas-Ayala et al. (2012) and Rajpurohit et al. (2013), respectively, while our typical error is ~ 140 K. See text for discussion.

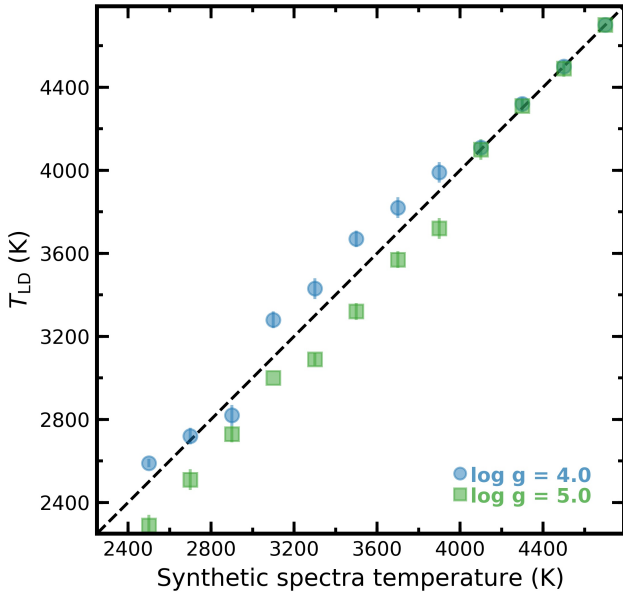


Figure 7. Line-depth temperature as function of synthetic spectra temperature with $\log g = 4.0$ (circles) and 5.0 (squares) dex. We determined the temperatures with a fixed $\log g$ of 4.5 dex. For synthetic spectra with $T_{\text{eff}} < 3100$ K, the determined temperature comes from the Al region, while the other from the OH region.

than 4.5 and viceversa. Stars with $\log g = 4.5$ will show no systematic offset in T_{eff} due to surface gravity assumptions.

4.1.3. Rotational velocity effects

As in the last section, we used synthetic spectra with different $v \sin i$ values to assess the uncertainty introduced by an erroneous $v \sin i$. We tested $\Delta v \sin i = 5 \text{ km s}^{-1}$ and our findings are shown in the Figure 8. For $T_{\text{eff}} < 3000$ K and $T_{\text{eff}} > 4000$ K the temperatures are less affected by a wrong $v \sin i$ value, with differences of the order of 20 K. The remaining temperatures appear cooler in average 130 K for fast rotators, while for slow rotators they are hotter by ~ 100 K, therefore we consider that a difference in $v \sin i$ of $\pm 5 \text{ km s}^{-1}$ from our calculated value has the effect of changing T_{eff} up to 120 K. Such an effect will increase the derived temperature if $v \sin i$ is underestimated and viceversa. Stars with $v \sin i$ determined to within $\pm 2 \text{ km s}^{-1}$ of the actual value, which is the case for much of our sample, will show minimal systematic offset in temperature due to $v \sin i$ errors.

4.1.4. Cumulative Uncertainty Budget

In the case that we properly match the observed star's properties to our model grid ($\log g = 4.5$, $[\text{Fe}/\text{H}] = 0.0$,

Table 2. Median T_{eff} and standard deviation, along with the temperature determined by PM13 = Pecaut & Mamajek (2013) and R13 = Rajpurohit et al. (2013) for each SpT. Stars with intermediate spectral classifications were not include.

SpT	# stars	$T_{\text{eff}} \pm \sigma$	PM13	R13
		(K)	(K)	(K)
K5	6	4165 ± 200	4410	–
K6	2	4120 ± 40^a	4230	–
K7	8	4090 ± 100	4070	–
M0	19	3870 ± 220	3870	3900
M1	10	3730 ± 130	3700	3700
M2	11	3480 ± 120	3550	3500
M3	14	3410 ± 90	3410	3300
M4	28	3315 ± 100	3200	3200
M5	19	3080 ± 120	3030	3000
M6	9	2950 ± 130	2850	2800
M7	7	2880 ± 200	2650	2700

^aThe average temperature and the difference between individual determinations is reported.

$v \sin i = 7 - 55 \text{ km s}^{-1}$, spectral resolution of 45,000 and no α -element enrichment) our T_{spec} uncertainties are driven by the calibration sample and are $\sim 140 \text{ K}$. To have an estimate of the systematic error on our temperature determinations, we considered three different sources of error: $[\text{Fe}/\text{H}]$, $\log g$ and $v \sin i$. Linearly interpolating from the previous error analysis to the typical uncertainties for $[\text{Fe}/\text{H}]$, $v \sin i$ and $\log g$ in our sample (which are 0.25, 3 km s^{-1} and 0.25, respectively) we find a systematic uncertainty as high as 120 K. For most of the stars in our sample, the errors presented in Table 1 should properly account for calibration errors and small deviations from the model grid. However, the systematic uncertainty of 120 K should be added for those objects with known outlier properties. From the examination of each contributing stellar parameter, temperature determinations can be further corrected for stars that have known properties that depart from the fixed values chosen in this study.

4.2. Line Depth Ratios for Temperature Determination

To support the broad applicability of our method, we obtained a mathematical expression that represents our temperature scale. We constructed a relation between T_{eff} and the line-depth ratio (LDR) in each region. The

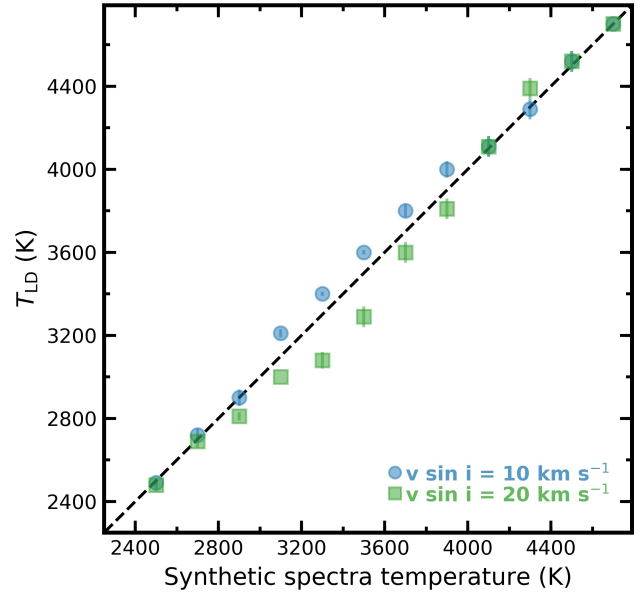


Figure 8. Line-depth temperatures as function of the synthetic spectra temperature with $v \sin i = 10$ (circles) and 20 km s^{-1} (squares). We determined the temperatures with a fixed $v \sin i$ of 15 km s^{-1} . For synthetic spectra with temperatures greater than 3100 K , the determined temperature comes from the Al region, while the rest come from the OH region.

LDR technique should be less sensitive to broadening processes that affect line-depths nearly equally, such as, resolution effects or veiling⁶ in Young Stellar Objects (YSOs).

4.2.1. LDR vs. T_{spec}

In Figure 9, we show T_{spec} as a function of the ratio between the line-depth of the peak and the Al I (right panel) and between the Fe I and OH (left panel) lines. Such relations show, as expected, a good correlation between temperature and LDR within the range of 3000-4000 K. However, both LDRs exhibit a plateau at the hot and cool ends of the temperature sequence. The plateau in the OH region is produced by the reduction of the flux in the OH line at $T_{\text{spec}} \sim 4200 \text{ K}$. In the Al region the cold temperature plateau is a result of the inability of the BT-Settl models to fully reproduce the ‘peak’ flux for temperatures below $\sim 3000 \text{ K}$ (Figure 2). Therefore we just consider the linear regime of both relations and fit a weighted line ($T_{\text{eff}} = aX + b$) between $\text{LDR}(\text{peak}/\text{Al}) > -0.5$ and $\text{LDR}(\text{Fe}/\text{OH}) < 1.5$. The coefficients of this linear fit are $m = 520$ and $b = 3230 \text{ K}$

⁶ The veiling is a continuum emission produce by the accretion of material onto the young star. This process reduces the depth of the photospheric lines.

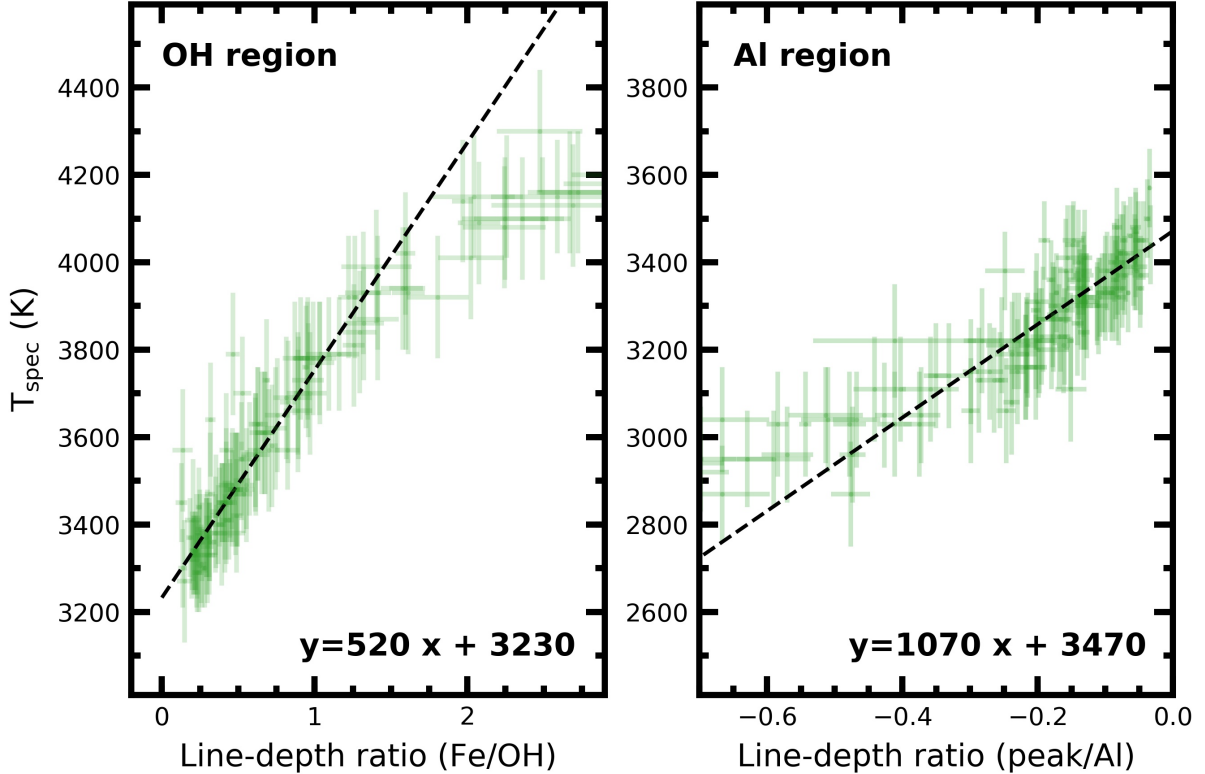


Figure 9. T_{spec} as function of LDR for both regions. The dashed line represents a linear fit to the data enclosed by $\text{LDR}(\text{Fe}/\text{OH}) < 1.5$ and $\text{LDR}(\text{peak}/\text{Al}) > -0.5$.

for the OH region, and $m = 1070$ and $b = 3470$ K for the Al region. The dispersion of the data around the fitted line is only ~ 70 K in both regions.

4.2.2. Testing our $T_{\text{spec}}\text{-LDR}$ scale on TWA members

The TW Hydrae Association (TWA) is a nearby (~ 60 pc; Zuckerman & Song 2004; Gaia Collaboration et al. (2018)), young ($\sim 7\text{--}10$ Myr; Ducourant et al. 2014; Herczeg & Hillenbrand 2015; Sokal et al. 2018) group of stars, discovered by Kastner et al. (1997). The Young Stellar Objects (YSOs) in TWA differ from the main-sequence stars in Table 1 mainly by differences in $\log g$ (~ 4.0) and stellar activity. The members of TWA allow us to test the capabilities and scope of our derived $T_{\text{spec}}\text{-LDR}$ relationship beyond the field sample for which it was calibrated.

We measured $\text{LDR}(\text{Fe}/\text{OH})$ in twelve TWA members, observed with IGRINS at Gemini South in 2018, to compute their respective LDR temperatures (T_{LDR}) according to our $T_{\text{spec}}\text{-LDR}$ relation. The results obtained are presented in Table 3 and compared with the previous determinations of Herczeg & Hillenbrand (2014) in Figure 10.

We find that there is a slight offset between T_{LDR} and the temperatures determined by Herczeg & Hillenbrand

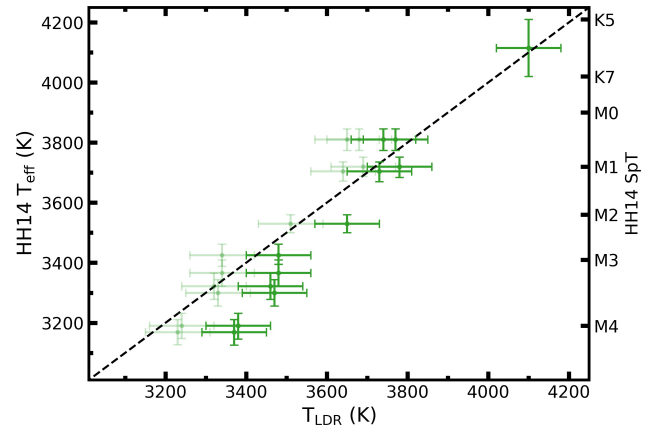


Figure 10. LDR temperatures compared with those determined by Herczeg & Hillenbrand (2014) for twelve members of TWA. The dashed line is the one-to-one relation, while the lighter points are the LDR temperatures corrected by 140 K ($T_{\text{LDR}} \leq 3700$ K) and 90 K ($3700 < T_{\text{LDR}} < 4000$ K) to account for $\log g$ differences between TWA and the calibration sample in this paper.

(2014). The offset at lower temperatures observed in Figure 10 is consistent with the findings of Figure 7, which implies that T_{LDR} will overestimate temperatures between 3100 and 3800 K for a young star with $\log g$ of

Table 3. LDR effective temperatures and its error, determined through our T_{spec} -LDR relations for the members of TWA. The error on the temperatures is of 80 K. Spectral types are from [Herczeg & Hillenbrand \(2014\)](#).

Star	SpT	LDR(Fe/OH)	T_{LDR} (K)
TWA 1	M0.5	0.98±0.06	3740
TWA 2	M2.2	0.81±0.02	3650
TWA 3A	M4.1	0.27±0.01	3370
TWA 3B	M4.0	0.28±0.01	3380
TWA 7	M3.2	0.48±0.04	3480
TWA 8A	M2.9	0.48±0.03	3480
TWA 9A	K6.0	1.66±0.03	4100
TWA 9B	M3.4	0.44±0.01	3460
TWA 13A	M1.1	0.96±0.03	3730
TWA 13B	M1.0	1.05±0.03	3780
TWA 23	M3.5	0.45±0.02	3470
TWA 25	M0.5	1.03±0.03	3770

4.0. From this test we can say that the presented relationships hold true for objects most like the model grid, and behave predictably near the parameters considered.

4.2.3. Employing LDR Method at Different Spectral Resolutions

The T_{spec} -LDR relation could also be employed for spectra with lower/higher spectral resolution, as long as the lines can be resolved and there is no excessive blending. To show this, we tested the relationships on synthetic spectra that were broadened to different spectral resolutions ($3,000 \leq R \leq 120,000$). This range in spectral resolution includes some available infrared spectrographs, such as, the CRyogenic high-resolution InfraRed Echelle Spectrograph (CRIRES; $R = 100,000$; [Kaeufl et al. 2004](#); [Follert et al. 2014](#)), the Calar Alto high-Resolution search for M dwarfs with Exoearths with Near-infrared and optical chelle Spectrographs (CARMENES, $R \sim 90,000$; [Quirrenbach et al. 2014](#), iSHELL ($R \sim 75,000$; [Rayner et al. 2016](#)), the Apache Point Observatory Galaxy Evolution Experiment ($R = 22,500$; [Majewski et al. 2016](#)), NIRSPEC at Keck Observatory ($R \sim 25,000$; [McLean et al. 1998](#); [Martin et al. 2018](#)), and X-shooter ($R \sim 12,000$; [Vernet et al. 2011](#)).

After broadening the synthetic spectra to the desired resolution, we added random Gaussian noise of 1% of

the median flux of each region and then computed line-depths and LDRs in the same fashion as for our observations. In the upper panels of [Figure 11](#), we display the LDR as a function of R , while in the lower ones are shown LDR divided by its error (σ_{LDR}). Together these plots help us to understand the limitations of our LDR method. In the OH region the cooler model ($T_{\text{eff}} = 3000$ K) is the more affected by R (for $R = 30,000$ the $\text{LDR} = 1.8 \times \sigma_{\text{LDR}}$), which we consider marginally useful since its value is not significantly different than the noise level. Nevertheless, $\text{LDR}(\text{Fe}/\text{OH})$ seems to be useful across the whole range in the remaining synthetic spectra with $T_{\text{eff}} = 3500$ and 4000 K. The $\text{LDR}(\text{peak}/\text{Al})$ is useful for $R \geq 10,000$ in synthetic spectra with $T_{\text{eff}} = 2500$ and 3000 K.

These results are not entirely surprising since low sensitivity to changes in spectral resolution is one of the benefits of the LDR technique, therefore our T_{spec} -LDR relationships should be applicable to any infrared spectrum with $R \gtrsim 10,000$. Even more, if the applicability of such relationships can be extend to YSOs, as our test with some members of TWA suggests, the T_{spec} -LDR relationship could become a powerful tool to characterize large samples of stars at different ages. This is especially critical because large spectral coverage permits the simultaneous determination of numerous stellar properties at a single epoch of observation, eliminating the need for coincident photometry and reducing the impacts of photospheric variability between epochs of observation.

4.3. Comments on individual stars

In this section we discuss a few stars in our sample with T_{eff} values in the literature. The goal of this section is to point out the limitations of our method as well as to highlight some interesting cases.

TRAPPIST-1 is a M8 dwarf which hosts seven Earth-sized planets, three of which are in the habitable zone ([Gillon et al. 2017](#)). [Filippazzo et al. \(2015\)](#), through a precise bolometric luminosity and radius estimate from evolutionary models, derived a semi-empirical T_{eff} for TRAPPIST-1 of 2557 ± 64 K. With a new measurement of the trigonometric parallax of TRAPPIST-1, [Van Grootel et al. \(2018\)](#) obtained an updated luminosity value, that they combine with revised radius estimates, to determine a $T_{\text{eff}} = 2516 \pm 41$ K. The last two temperatures are in good agreement within the uncertainties, however, more recently, [Rajpurohit et al. \(2018a\)](#) derived a cooler temperature (2400 ± 100 K) for TRAPPIST-1. Our T_{spec} for TRAPPIST-1 is 2870 ± 120 K, which is much hotter than all the pre-

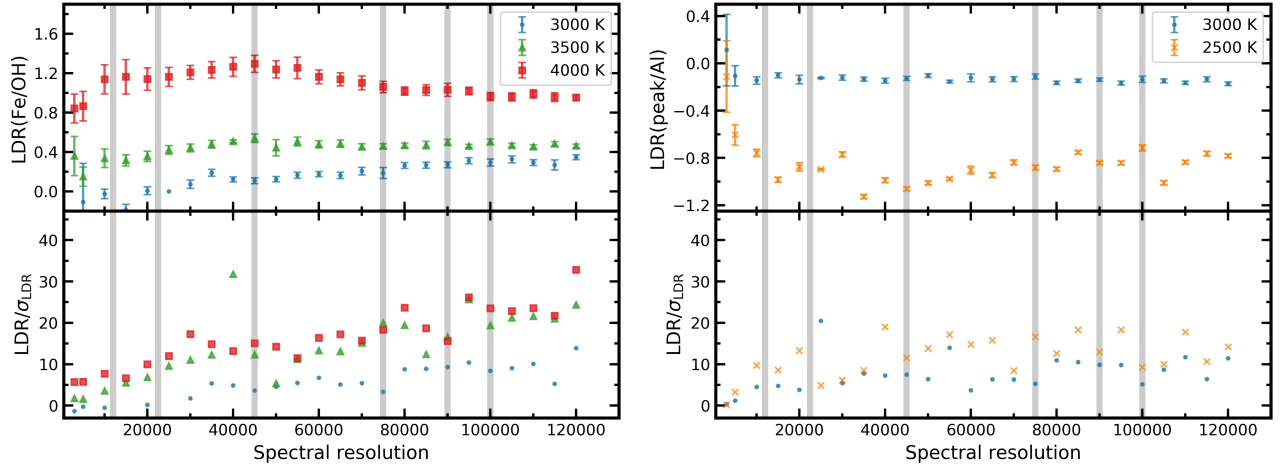


Figure 11. Line-depth ratios of synthetic spectra with $T_{\text{eff}} = 2500$ K (crosses), $T_{\text{eff}} = 3000$ K (circles), $T_{\text{eff}} = 3500$ K (triangles) and $T_{\text{eff}} = 4000$ K (squares) broadened to different resolutions (upper panels). The gray vertical lines represents spectral resolutions of different infrared spectrographs: X-shooter ($R = 12,000$), APOGEE ($R = 22,500$), IGRINS ($R = 45,000$), iSHELL ($R = 75,000$), CARMENES ($R = 90,000$) and CRIRES ($R = 100,000$). The lower panels is the LDR divide by the uncertainty.

vious determinations. This large discrepancy ($\gtrsim 300$ K) could be caused by two effects, the first is the inability of the models to properly reproduce the peak of flux in the Al region below 3000 K, and as a result yielding hotter line-depth temperatures. The second is the fact that the color-Temperature relation of Mann et al. (2015), which we used to calibrate our temperature scale, is no longer valid at SpT of M8 or later and will produce less accurate temperatures. Recently, Rabus et al. (2019) determined stellar radii, effective temperatures, masses and luminosities for low-mass dwarfs by means of interferometric measurements of stellar diameters and parallaxes. Their results showed a discontinuity in the T_{eff} -radius around 3200 K, therefore, the Mann et al. temperature sequence, and thus our T_{spec} , for temperatures cooler than 3200 K would be affected by this discontinuity. As showed by Rabus et al. (2019), the temperatures of Mann et al. (2015) are overestimates by about $\sim 6\%$ for the coolest objects (about 2800 K). If we take into account that overestimation, the T_{spec} for TRAPPIST-1 is then 2700 ± 120 , which is still hotter than previous determinations. If we omit the calibration of T_{LD} for TRAPPIST-1, the temperature derived by our line-depth method is 2500 ± 50 K, which is in agreement with previous determinations. Additionally, if we compute $\text{LDR}(\text{peak}/\text{Al})$ of TRAPPIST-1 and used the previous discussed T_{spec} -LDR relation, we obtain a T_{LDR} of 2430 ± 120 K, which is again in better agreement with previous determinations. These differences support the previous determination that our calibration is not yet reliable below ~ 3000 K.

Wolf 359 is a M6 star for which Mann et al. (2015) determined a temperature of 2818 ± 60 K, in agreement with Rajpurohit et al. (2013) ($T_{\text{eff}} = 2800 \pm 100$ K), Basri et al. (2000) ($T_{\text{eff}} = 2800$ K), and Rojas-Ayala et al. (2012) ($T_{\text{eff}} = 2887 \pm 20$ K). Our temperature ($T_{\text{spec}} = 3030 \pm 120$ K) is within the uncertainties, nevertheless, the LDR temperature ($T_{\text{LDR}} = 2840 \pm 70$ K) results in a better agreement. Contrary, to these numbers, Filippazzo et al. (2015) determined a much cooler temperature ($T_{\text{eff}} = 2517 \pm 81$ K), which is about the expected temperature for a M8 star according to the SpT- T_{eff} scale of Pecaut & Mamajek (2013).

UCAC4 527-008015 is a M4.5 dwarf member of the Hyades cluster, that is orbited by a Neptune-size planet (Mann et al. 2016). Mann et al. (2016) compare an optical spectrum with BT-Settl models and derive $T_{\text{eff}} = 3180 \pm 60$ K, which is within the uncertainties of our determined value $T_{\text{spec}} = 3280 \pm 120$ K.

Barnard's star is a M4 dwarf (Kirkpatrick et al. 1991) that hosts a super-Earth candidate (Ribas et al. 2018). We determined for Barnard's star a temperature of 3220 ± 110 K, which is in good agreement with previous determinations, such as, Mann et al. (2015) ($T_{\text{eff}} = 3228 \pm 60$ K), Boyajian et al. (2012) ($T_{\text{eff}} = 3222 \pm 10$ K), Rojas-Ayala et al. (2012) ($T_{\text{eff}} = 3266 \pm 29$ K), and Dawson & De Robertis (2004) ($T_{\text{eff}} = 3134 \pm 102$ K).

YY Gem is a double-lined eclipsing binary (Joy & Sanford 1926; Bopp 1974). Veeder (1974) deter-

mined a temperature of 3741 ± 150 K from photometric colors for YY Gem. More recently, Torres & Ribas (2002) obtained $T_{\text{eff}} = 3820 \pm 100$ K, from an analysis of light curves and optical spectra, while Eker et al. (2015) through the Stefan-Boltzmann law obtained $T_{\text{eff}} = 3874 \pm 271$ K. The double-lined spectroscopic binary features of YY Gem are present in our IGRINS spectrum, crowding the OH region and complicating the identification of the Fe I and OH lines. Despite that, in the Na I line region (used to estimate the radial velocity) both components are easily identifiable and they seem to be of similar SpT. Additionally, the high rotational velocity of YY Gem ($v \sin i = 47 \text{ km s}^{-1}$) complicates the determination of T_{eff} . We obtained $T_{\text{spec}} = 4300 \pm 140$ K and if we correct our spectra to the radial velocity of the other component the resultant temperature is $T_{\text{eff}} = 4380 \pm 130$ K. These differences support the previous determination that our calibration is not yet reliable above ~ 4000 K.

In the above analysis and discussion, we have shown that T_{spec} is in agreement with previous determinations within the range of 3000-4000 K stars. The more ‘typical’ a star is to our assumed parameters ($\log g = 4.5$, $[\text{Fe}/\text{H}] = 0.0$, $v \sin i = 7 - 55 \text{ km s}^{-1}$, spectral resolution of 45,000 and no α -element enrichment) the more accurate and precise the derived temperatures.

5. SUMMARY AND CONCLUSIONS

We have determined T_{spec} for 254 K and M dwarfs using line-depths measured in high-resolution H-band spectra from IGRINS and the CFIST version of the BT-Settl models. Our temperature scale was compared with and calibrated, through a model-independent ($r - J$) color-Temperature relation, to the temperature scale of Mann et al. (2015), resulting in good agreement with previous determinations for objects between 4000-3000 K ($\sim \text{K8-M5}$). We employed model spectra to investigate the stability of the temperature scale to changes in $[\text{Fe}/\text{H}]$, $\log g$, and $v \sin i$ finding just a slight trend with $[\text{Fe}/\text{H}]$, and offsets for non-typical $\log g$ or incorrect $v \sin i$ measurements. The method presented in this paper allows for the determination of accurate and precise temperatures consistent with the Mann et al. (2015) temperature sequence, however, the BT-Settl model temperatures are easily recoverable and they can be calibrated with any other desired temperature scale. We also present T_{spec} -LDR relationships, which we will

use to guide our primary scientific goal of accurately and precisely determining stellar parameters for the IGRINS YSO Survey. The temperature and model characterization presented here is a major step towards that goal. Finally, we show that T_{spec} -LDR relationships are insensitive to changes in spectral resolution $R \gtrsim 10,000$ and can be extended to data taken by other high-resolution, near-infrared spectrographs.

We thank the anonymous referee for helping us clarify our methods and develop the discussion of our analysis. This work used the Immersion Grating Infrared Spectrometer (IGRINS) that was developed under a collaboration between the University of Texas at Austin and the Korea Astronomy and Space Science Institute (KASI) with the financial support of the US National Science Foundation under grants AST-1229522 and AST-1702267, of the University of Texas at Austin, and of the Korean GMT Project of KASI. This paper includes data taken at The McDonald Observatory of The University of Texas at Austin. These results made use of the Discovery Channel Telescope at Lowell Observatory. Lowell is a private, non-profit institution dedicated to astrophysical research and public appreciation of astronomy and operates the DCT in partnership with Boston University, the University of Maryland, the University of Toledo, Northern Arizona University and Yale University. Based on observations obtained at the Gemini Observatory, which is operated by the Association of Universities for Research in Astronomy, Inc., under a cooperative agreement with the NSF on behalf of the Gemini partnership: the National Science Foundation (United States), the National Research Council (Canada), CONICYT (Chile), Ministerio de Ciencia, Tecnología e Innovación Productiva (Argentina), and Ministério da Ciência, Tecnologia e Inovação (Brazil). This research has made use of the SIMBAD database, operated at CDS, Strasbourg, France. This research was made possible through the use of the AAVSO Photometric All-Sky Survey (APASS), funded by the Robert Martin Ayers Sciences Fund.

Software: IGRINS pipeline (v2.1 alpha 3; Lee, Gullikson, & Kaplan 2017), PHOENIX (Hauschildt et al. 1997), PyAstronomy (<https://github.com/sczesla/PyAstronomy>)

REFERENCES

- Aberasturi, M., Caballero, J. A., Montesinos, B., et al. 2014, AJ, 148, 36, doi: [10.1088/0004-6256/148/2/36](https://doi.org/10.1088/0004-6256/148/2/36)
- Allard, F., Homeier, D., Freytag, B., et al. 2013, Memorie della Societa Astronomica Italiana Supplementi, 24, 128. <https://arxiv.org/abs/1302.6559>

- Alonso, A., Arribas, S., & Martínez-Roger, C. 1996, *A&A*, 313, 873
- Alonso-Floriano, F. J., Morales, J. C., Caballero, J. A., et al. 2015, *A&A*, 577, A128, doi: [10.1051/0004-6361/201525803](https://doi.org/10.1051/0004-6361/201525803)
- Asplund, M., Grevesse, N., Sauval, A. J., & Scott, P. 2009, *ARA&A*, 47, 481, doi: [10.1146/annurev.astro.46.060407.145222](https://doi.org/10.1146/annurev.astro.46.060407.145222)
- Baraffe, I., Homeier, D., Allard, F., & Chabrier, G. 2015, *A&A*, 577, A42, doi: [10.1051/0004-6361/201425481](https://doi.org/10.1051/0004-6361/201425481)
- Basri, G., Mohanty, S., Allard, F., et al. 2000, *ApJ*, 538, 363, doi: [10.1086/309095](https://doi.org/10.1086/309095)
- Benedict, G. F., Tanner, A. M., Cargile, P. A., & Ciardi, D. R. 2014, *AJ*, 148, 108, doi: [10.1088/0004-6256/148/6/108](https://doi.org/10.1088/0004-6256/148/6/108)
- Berger, D. H., Gies, D. R., McAlister, H. A., et al. 2006, *ApJ*, 644, 475, doi: [10.1086/503318](https://doi.org/10.1086/503318)
- Bessell, M. S. 1991, *AJ*, 101, 662, doi: [10.1086/115714](https://doi.org/10.1086/115714)
- Biazzo, K., Pasquini, L., Girardi, L., et al. 2007, *A&A*, 475, 981, doi: [10.1051/0004-6361:20077374](https://doi.org/10.1051/0004-6361:20077374)
- Bidelman, W. P. 1985, *ApJS*, 59, 197, doi: [10.1086/191069](https://doi.org/10.1086/191069)
- Bochanski, J. J., Hawley, S. L., Covey, K. R., et al. 2010, *AJ*, 139, 2679, doi: [10.1088/0004-6256/139/6/2679](https://doi.org/10.1088/0004-6256/139/6/2679)
- Bonfils, X., Gillon, M., Udry, S., et al. 2012, *A&A*, 546, A27, doi: [10.1051/0004-6361/201219623](https://doi.org/10.1051/0004-6361/201219623)
- Bopp, B. W. 1974, *ApJ*, 193, 389, doi: [10.1086/153174](https://doi.org/10.1086/153174)
- Bouy, H., & Martín, E. L. 2009, *A&A*, 504, 981, doi: [10.1051/0004-6361/200811088](https://doi.org/10.1051/0004-6361/200811088)
- Bowler, B. P., Liu, M. C., Shkolnik, E. L., & Tamura, M. 2015, *ApJS*, 216, 7, doi: [10.1088/0067-0049/216/1/7](https://doi.org/10.1088/0067-0049/216/1/7)
- Boyajian, T. S., von Braun, K., van Belle, G., et al. 2012, *ApJ*, 757, 112, doi: [10.1088/0004-637X/757/2/112](https://doi.org/10.1088/0004-637X/757/2/112)
- Caffau, E., Ludwig, H.-G., Steffen, M., Freytag, B., & Bonifacio, P. 2011, *SoPh*, 268, 255, doi: [10.1007/s11207-010-9541-4](https://doi.org/10.1007/s11207-010-9541-4)
- Casagrande, L., Flynn, C., & Bessell, M. 2008, *MNRAS*, 389, 585, doi: [10.1111/j.1365-2966.2008.13573.x](https://doi.org/10.1111/j.1365-2966.2008.13573.x)
- Casagrande, L., Portinari, L., & Flynn, C. 2006, *MNRAS*, 373, 13, doi: [10.1111/j.1365-2966.2006.10999.x](https://doi.org/10.1111/j.1365-2966.2006.10999.x)
- Casagrande, L., Ramírez, I., Meléndez, J., Bessell, M., & Asplund, M. 2010, *A&A*, 512, A54, doi: [10.1051/0004-6361/200913204](https://doi.org/10.1051/0004-6361/200913204)
- Cenarro, A. J., Peletier, R. F., Sánchez-Blázquez, P., et al. 2007, *MNRAS*, 374, 664, doi: [10.1111/j.1365-2966.2006.11196.x](https://doi.org/10.1111/j.1365-2966.2006.11196.x)
- Chabrier, G. 2005, in *Astrophysics and Space Science Library*, Vol. 327, *The Initial Mass Function 50 Years Later*, ed. E. Corbelli, F. Palla, & H. Zinnecker, 41
- Claret, A., Hauschildt, P. H., & Witte, S. 2012, *A&A*, 546, A14, doi: [10.1051/0004-6361/201219849](https://doi.org/10.1051/0004-6361/201219849)
- Cutri, R. M., Skrutskie, M. F., van Dyk, S., et al. 2003, *VizieR Online Data Catalog*, II/246
- Davison, C. L., White, R. J., Henry, T. J., et al. 2015, *AJ*, 149, 106, doi: [10.1088/0004-6256/149/3/106](https://doi.org/10.1088/0004-6256/149/3/106)
- Dawson, P. C., & De Robertis, M. M. 2004, *AJ*, 127, 2909, doi: [10.1086/383289](https://doi.org/10.1086/383289)
- Ducourant, C., Teixeira, R., Galli, P. A. B., et al. 2014, *A&A*, 563, A121, doi: [10.1051/0004-6361/201322075](https://doi.org/10.1051/0004-6361/201322075)
- Eker, Z., Soyduğan, F., Soyduğan, E., et al. 2015, *AJ*, 149, 131, doi: [10.1088/0004-6256/149/4/131](https://doi.org/10.1088/0004-6256/149/4/131)
- Fekel, F. C., & Bopp, B. W. 1993, *ApJL*, 419, L89, doi: [10.1086/187144](https://doi.org/10.1086/187144)
- Filippazzo, J. C., Rice, E. L., Faherty, J., et al. 2015, *ApJ*, 810, 158, doi: [10.1088/0004-637X/810/2/158](https://doi.org/10.1088/0004-637X/810/2/158)
- Follert, R., Dorn, R. J., Oliva, E., et al. 2014, in *Proc. SPIE*, Vol. 9147, *Ground-based and Airborne Instrumentation for Astronomy V*, 914719
- Fukue, K., Matsunaga, N., Yamamoto, R., et al. 2015, *ApJ*, 812, 64, doi: [10.1088/0004-637X/812/1/64](https://doi.org/10.1088/0004-637X/812/1/64)
- Gagné, J., Faherty, J. K., Cruz, K. L., et al. 2015, *ApJS*, 219, 33, doi: [10.1088/0067-0049/219/2/33](https://doi.org/10.1088/0067-0049/219/2/33)
- Gaia Collaboration, Brown, A. G. A., Vallenari, A., et al. 2018, *A&A*, 616, A1, doi: [10.1051/0004-6361/201833051](https://doi.org/10.1051/0004-6361/201833051)
- García Pérez, A. E., Allende Prieto, C., Holtzman, J. A., et al. 2016, *AJ*, 151, 144, doi: [10.3847/0004-6256/151/6/144](https://doi.org/10.3847/0004-6256/151/6/144)
- Gigoyan, K. S., & Mickaelian, A. M. 2012, *MNRAS*, 419, 3346, doi: [10.1111/j.1365-2966.2011.19974.x](https://doi.org/10.1111/j.1365-2966.2011.19974.x)
- Gillon, M., Jehin, E., Lederer, S. M., et al. 2016, *Nature*, 533, 221, doi: [10.1038/nature17448](https://doi.org/10.1038/nature17448)
- Gillon, M., Triaud, A. H. M. J., Demory, B.-O., et al. 2017, *Nature*, 542, 456, doi: [10.1038/nature21360](https://doi.org/10.1038/nature21360)
- Gomes, J. I., Pinfield, D. J., Marocco, F., et al. 2013, *MNRAS*, 431, 2745, doi: [10.1093/mnras/stt371](https://doi.org/10.1093/mnras/stt371)
- Gray, D. F., & Johanson, H. L. 1991, *PASP*, 103, 439, doi: [10.1086/132839](https://doi.org/10.1086/132839)
- Gray, R. O., Corbally, C. J., Garrison, R. F., McFadden, M. T., & Robinson, P. E. 2003, *AJ*, 126, 2048, doi: [10.1086/378365](https://doi.org/10.1086/378365)
- Hauschildt, P. H., Allard, F., Alexander, D. R., & Baron, E. 1997, *ApJ*, 488, 428, doi: [10.1086/304674](https://doi.org/10.1086/304674)
- Hawkins, K., Jofré, P., Heiter, U., et al. 2016, *A&A*, 592, A70, doi: [10.1051/0004-6361/201628268](https://doi.org/10.1051/0004-6361/201628268)
- Henden, A. A., Levine, S. E., Terrell, D., Smith, T. C., & Welch, D. 2012, *Journal of the American Association of Variable Star Observers (JAAVSO)*, 40, 430
- Henry, T. J., Walkowicz, L. M., Barto, T. C., & Golimowski, D. A. 2002, *AJ*, 123, 2002, doi: [10.1086/339315](https://doi.org/10.1086/339315)

- Herczeg, G. J., & Hillenbrand, L. A. 2014, *ApJ*, 786, 97, doi: [10.1088/0004-637X/786/2/97](https://doi.org/10.1088/0004-637X/786/2/97)
- . 2015, *ApJ*, 808, 23, doi: [10.1088/0004-637X/808/1/23](https://doi.org/10.1088/0004-637X/808/1/23)
- Horne, K. 1986, *PASP*, 98, 609, doi: [10.1086/131801](https://doi.org/10.1086/131801)
- Houk, N., & Cowley, A. P. 1975, University of Michigan Catalogue of two-dimensional spectral types for the HD stars. Volume I. Declinations -90_ to -53.f0.
- Houk, N., & Swift, C. 1999, in *Michigan Spectral Survey*, Ann Arbor, Dep. Astron., Univ. Michigan, Vol. 5, p. 0 (1999), Vol. 5, 0
- Husser, T.-O., Wende-von Berg, S., Dreizler, S., et al. 2013, *A&A*, 553, A6, doi: [10.1051/0004-6361/201219058](https://doi.org/10.1051/0004-6361/201219058)
- Joy, A. H., & Abt, H. A. 1974, *ApJS*, 28, 1, doi: [10.1086/190307](https://doi.org/10.1086/190307)
- Joy, A. H., & Sanford, R. F. 1926, *ApJ*, 64, doi: [10.1086/143009](https://doi.org/10.1086/143009)
- Kaeuffl, H.-U., Ballester, P., Biereichel, P., et al. 2004, in *Proc. SPIE*, Vol. 5492, Ground-based Instrumentation for Astronomy, ed. A. F. M. Moorwood & M. Iye, 1218–1227
- Kastner, J. H., Zuckerman, B., Weintraub, D. A., & Forveille, T. 1997, *Science*, 277, 67, doi: [10.1126/science.277.5322.67](https://doi.org/10.1126/science.277.5322.67)
- Keenan, P. C., & McNeil, R. C. 1989, *ApJS*, 71, 245, doi: [10.1086/191373](https://doi.org/10.1086/191373)
- Kesseli, A. Y., Muirhead, P. S., Mann, A. W., & Mace, G. 2018, *AJ*, 155, 225, doi: [10.3847/1538-3881/aabccb](https://doi.org/10.3847/1538-3881/aabccb)
- Kirkpatrick, J. D., Henry, T. J., & McCarthy, Jr., D. W. 1991, *ApJS*, 77, 417, doi: [10.1086/191611](https://doi.org/10.1086/191611)
- Koen, C., Kilkenny, D., van Wyk, F., & Marang, F. 2010, *MNRAS*, 403, 1949, doi: [10.1111/j.1365-2966.2009.16182.x](https://doi.org/10.1111/j.1365-2966.2009.16182.x)
- Kraus, A. L., Shkolnik, E. L., Allers, K. N., & Liu, M. C. 2014, *AJ*, 147, 146, doi: [10.1088/0004-6256/147/6/146](https://doi.org/10.1088/0004-6256/147/6/146)
- Kurucz, R. L. 1979, *ApJS*, 40, 1, doi: [10.1086/190589](https://doi.org/10.1086/190589)
- Law, N. M., Hodgkin, S. T., & Mackay, C. D. 2008, *MNRAS*, 384, 150, doi: [10.1111/j.1365-2966.2007.12675.x](https://doi.org/10.1111/j.1365-2966.2007.12675.x)
- Lee, J.-J., Gullikson, K., & Kaplan, K. 2017, *igrins/plp* 2.2.0. Zenodo, doi: [10.5281/zenodo.845059](https://doi.org/10.5281/zenodo.845059)
- Lépine, S., Hilton, E. J., Mann, A. W., et al. 2013, *AJ*, 145, 102, doi: [10.1088/0004-6256/145/4/102](https://doi.org/10.1088/0004-6256/145/4/102)
- Mace, G., Kim, H., Jaffe, D. T., et al. 2016, in *Proc. SPIE*, Vol. 9908, Ground-based and Airborne Instrumentation for Astronomy VI, 99080C
- Mace, G., Sokal, K., Lee, J.-J., et al. 2018, in *Society of Photo-Optical Instrumentation Engineers (SPIE) Conference Series*, Vol. 10702, Society of Photo-Optical Instrumentation Engineers (SPIE) Conference Series, 107020Q
- Majewski, S. R., APOGEE Team, & APOGEE-2 Team. 2016, *Astronomische Nachrichten*, 337, 863, doi: [10.1002/asna.201612387](https://doi.org/10.1002/asna.201612387)
- Mann, A. W., Brewer, J. M., Gaidos, E., Lépine, S., & Hilton, E. J. 2013a, *AJ*, 145, 52, doi: [10.1088/0004-6256/145/2/52](https://doi.org/10.1088/0004-6256/145/2/52)
- Mann, A. W., Deacon, N. R., Gaidos, E., et al. 2014, *AJ*, 147, 160, doi: [10.1088/0004-6256/147/6/160](https://doi.org/10.1088/0004-6256/147/6/160)
- Mann, A. W., Feiden, G. A., Gaidos, E., Boyajian, T., & von Braun, K. 2015, *ApJ*, 804, 64, doi: [10.1088/0004-637X/804/1/64](https://doi.org/10.1088/0004-637X/804/1/64)
- Mann, A. W., Gaidos, E., & Ansdell, M. 2013b, *ApJ*, 779, 188, doi: [10.1088/0004-637X/779/2/188](https://doi.org/10.1088/0004-637X/779/2/188)
- Mann, A. W., Gaidos, E., Mace, G. N., et al. 2016, *ApJ*, 818, 46, doi: [10.3847/0004-637X/818/1/46](https://doi.org/10.3847/0004-637X/818/1/46)
- Mann, A. W., Dupuy, T., Kraus, A. L., et al. 2018, *ArXiv e-prints*. <https://arxiv.org/abs/1811.06938>
- Martin, E. C., Fitzgerald, M. P., McLean, I. S., et al. 2018, in *Society of Photo-Optical Instrumentation Engineers (SPIE) Conference Series*, Vol. 10702, Ground-based and Airborne Instrumentation for Astronomy VII, 107020A
- Masana, E., Jordi, C., & Ribas, I. 2006, *A&A*, 450, 735, doi: [10.1051/0004-6361:20054021](https://doi.org/10.1051/0004-6361:20054021)
- McLean, I. S., Becklin, E. E., Bendiksen, O., et al. 1998, in *Proc. SPIE*, Vol. 3354, Infrared Astronomical Instrumentation, ed. A. M. Fowler, 566–578
- Mera, D., Chabrier, G., & Baraffe, I. 1996, *ApJL*, 459, L87, doi: [10.1086/309952](https://doi.org/10.1086/309952)
- Montagnier, G., Ségransan, D., Beuzit, J.-L., et al. 2006, *A&A*, 460, L19, doi: [10.1051/0004-6361:20066120](https://doi.org/10.1051/0004-6361:20066120)
- Morton, D. C. 1991, *ApJS*, 77, 119, doi: [10.1086/191601](https://doi.org/10.1086/191601)
- Nesterov, V. V., Kuzmin, A. V., Ashimbaeva, N. T., et al. 1995, *A&AS*, 110
- Newton, E. R., Charbonneau, D., Irwin, J., et al. 2014, *AJ*, 147, 20, doi: [10.1088/0004-6256/147/1/20](https://doi.org/10.1088/0004-6256/147/1/20)
- Newton, E. R., Charbonneau, D., Irwin, J., & Mann, A. W. 2015, *ApJ*, 800, 85, doi: [10.1088/0004-637X/800/2/85](https://doi.org/10.1088/0004-637X/800/2/85)
- Park, C., Jaffe, D. T., Yuk, I.-S., et al. 2014, in *Proc. SPIE*, Vol. 9147, Ground-based and Airborne Instrumentation for Astronomy V, 91471D
- Park, S., Lee, J.-E., Kang, W., et al. 2018, *ApJS*, 238, 29, doi: [10.3847/1538-4365/aadd14](https://doi.org/10.3847/1538-4365/aadd14)
- Passegger, V. M., Reiners, A., Jeffers, S. V., et al. 2018, *A&A*, 615, A6, doi: [10.1051/0004-6361/201732312](https://doi.org/10.1051/0004-6361/201732312)
- Pecaut, M. J., & Mamajek, E. E. 2013, *ApJS*, 208, 9, doi: [10.1088/0067-0049/208/1/9](https://doi.org/10.1088/0067-0049/208/1/9)
- Pesch, P., & Bidelman, W. 1997, *PASP*, 109, 643, doi: [10.1086/133926](https://doi.org/10.1086/133926)
- Prato, L., Simon, M., Mazeh, T., et al. 2002, *ApJ*, 569, 863, doi: [10.1086/339397](https://doi.org/10.1086/339397)

- Prugniel, P., Vauglin, I., & Koleva, M. 2011, *A&A*, 531, A165, doi: [10.1051/0004-6361/201116769](https://doi.org/10.1051/0004-6361/201116769)
- Quirrenbach, A., Amado, P. J., Caballero, J. A., et al. 2014, in *Proc. SPIE*, Vol. 9147, Ground-based and Airborne Instrumentation for Astronomy V, 91471F
- Rabus, M., Lachaume, R., Jordán, A., et al. 2019, *MNRAS*, 484, 2674, doi: [10.1093/mnras/sty3430](https://doi.org/10.1093/mnras/sty3430)
- Rajpurohit, A. S., Allard, F., Rajpurohit, S., et al. 2018a, *A&A*, 620, A180, doi: [10.1051/0004-6361/201833500](https://doi.org/10.1051/0004-6361/201833500)
- Rajpurohit, A. S., Allard, F., Teixeira, G. D. C., et al. 2018b, *A&A*, 610, A19, doi: [10.1051/0004-6361/201731507](https://doi.org/10.1051/0004-6361/201731507)
- Rajpurohit, A. S., Reylé, C., Allard, F., et al. 2013, *A&A*, 556, A15, doi: [10.1051/0004-6361/201321346](https://doi.org/10.1051/0004-6361/201321346)
- Rayner, J., Tokunaga, A., Jaffe, D., et al. 2016, in *Society of Photo-Optical Instrumentation Engineers (SPIE) Conference Series*, Vol. 9908, Ground-based and Airborne Instrumentation for Astronomy VI, 99088A
- Reid, I. N., Cruz, K. L., & Allen, P. R. 2007, *AJ*, 133, 2825, doi: [10.1086/517914](https://doi.org/10.1086/517914)
- Reid, I. N., & Gizis, J. E. 1997, *AJ*, 113, 2246, doi: [10.1086/118436](https://doi.org/10.1086/118436)
- Reid, I. N., & Walkowicz, L. M. 2006, *PASP*, 118, 671, doi: [10.1086/503446](https://doi.org/10.1086/503446)
- Reid, I. N., Cruz, K. L., Allen, P., et al. 2004, *AJ*, 128, 463, doi: [10.1086/421374](https://doi.org/10.1086/421374)
- Reylé, C., Robin, A. C., Scholz, R.-D., & Irwin, M. 2002, *A&A*, 390, 491, doi: [10.1051/0004-6361:20020667](https://doi.org/10.1051/0004-6361:20020667)
- Riaz, B., Gizis, J. E., & Harvin, J. 2006, *AJ*, 132, 866, doi: [10.1086/505632](https://doi.org/10.1086/505632)
- Ribas, I., Tuomi, M., Reiners, A., et al. 2018, *Nature*, 563, 365, doi: [10.1038/s41586-018-0677-y](https://doi.org/10.1038/s41586-018-0677-y)
- Rojas-Ayala, B., Covey, K. R., Muirhead, P. S., & Lloyd, J. P. 2012, *ApJ*, 748, 93, doi: [10.1088/0004-637X/748/2/93](https://doi.org/10.1088/0004-637X/748/2/93)
- Santos, N. C., Israelian, G., & Mayor, M. 2000, *A&A*, 363, 228
- Santos, N. C., Sousa, S. G., Mortier, A., et al. 2013, *A&A*, 556, A150, doi: [10.1051/0004-6361/201321286](https://doi.org/10.1051/0004-6361/201321286)
- Schlieder, J. E., Lépine, S., Rice, E., et al. 2012a, *AJ*, 143, 114, doi: [10.1088/0004-6256/143/5/114](https://doi.org/10.1088/0004-6256/143/5/114)
- Schlieder, J. E., Lépine, S., & Simon, M. 2012b, *AJ*, 143, 80, doi: [10.1088/0004-6256/143/4/80](https://doi.org/10.1088/0004-6256/143/4/80)
- Schmidt, S. J., Cruz, K. L., Bongiorno, B. J., Liebert, J., & Reid, I. N. 2007, *AJ*, 133, 2258, doi: [10.1086/512158](https://doi.org/10.1086/512158)
- Scholz, R.-D., Meusinger, H., & Jahrei, H. 2005, *A&A*, 442, 211, doi: [10.1051/0004-6361:20053004](https://doi.org/10.1051/0004-6361:20053004)
- Ségransan, D., Kervella, P., Forveille, T., & Queloz, D. 2003, *A&A*, 397, L5, doi: [10.1051/0004-6361:20021714](https://doi.org/10.1051/0004-6361:20021714)
- Sharma, K., Prugniel, P., & Singh, H. P. 2016, *A&A*, 585, A64, doi: [10.1051/0004-6361/201526111](https://doi.org/10.1051/0004-6361/201526111)
- Shkolnik, E., Liu, M. C., & Reid, I. N. 2009, *ApJ*, 699, 649, doi: [10.1088/0004-637X/699/1/649](https://doi.org/10.1088/0004-637X/699/1/649)
- Sokal, K. R., Deen, C. P., Mace, G. N., et al. 2018, *ApJ*, 853, 120, doi: [10.3847/1538-4357/aaa1e4](https://doi.org/10.3847/1538-4357/aaa1e4)
- Sousa, S. G., Santos, N. C., Israelian, G., Mayor, M., & Udry, S. 2011, *A&A*, 533, A141, doi: [10.1051/0004-6361/201117699](https://doi.org/10.1051/0004-6361/201117699)
- Sousa, S. G., Santos, N. C., Mayor, M., et al. 2008, *A&A*, 487, 373, doi: [10.1051/0004-6361:200809698](https://doi.org/10.1051/0004-6361:200809698)
- Stephenson, C. B. 1986a, *AJ*, 91, 144, doi: [10.1086/113994](https://doi.org/10.1086/113994)
- . 1986b, *AJ*, 92, 139, doi: [10.1086/114146](https://doi.org/10.1086/114146)
- Taniguchi, D., Matsunaga, N., Kobayashi, N., et al. 2018, *MNRAS*, 473, 4993, doi: [10.1093/mnras/stx2691](https://doi.org/10.1093/mnras/stx2691)
- Terrien, R. C., Mahadevan, S., Bender, C. F., Deshpande, R., & Robertson, P. 2015, *ApJL*, 802, L10, doi: [10.1088/2041-8205/802/1/L10](https://doi.org/10.1088/2041-8205/802/1/L10)
- Torres, C. A. O., Quast, G. R., da Silva, L., et al. 2006, *A&A*, 460, 695, doi: [10.1051/0004-6361:20065602](https://doi.org/10.1051/0004-6361:20065602)
- Torres, G., & Ribas, I. 2002, *ApJ*, 567, 1140, doi: [10.1086/338587](https://doi.org/10.1086/338587)
- Tsantaki, M., Sousa, S. G., Adibekyan, V. Z., et al. 2013, *A&A*, 555, A150, doi: [10.1051/0004-6361/201321103](https://doi.org/10.1051/0004-6361/201321103)
- Van Grootel, V., Fernandes, C. S., Gillon, M., et al. 2018, *ApJ*, 853, 30, doi: [10.3847/1538-4357/aaa023](https://doi.org/10.3847/1538-4357/aaa023)
- Veeder, G. J. 1974, *AJ*, 79, 1056, doi: [10.1086/111653](https://doi.org/10.1086/111653)
- Vernet, J., Dekker, H., D’Odorico, S., et al. 2011, *A&A*, 536, A105, doi: [10.1051/0004-6361/201117752](https://doi.org/10.1051/0004-6361/201117752)
- Veyette, M. J., Muirhead, P. S., Mann, A. W., et al. 2017, *ApJ*, 851, 26, doi: [10.3847/1538-4357/aa96aa](https://doi.org/10.3847/1538-4357/aa96aa)
- von Braun, K., Boyajian, T. S., van Belle, G. T., et al. 2014, *MNRAS*, 438, 2413, doi: [10.1093/mnras/stt2360](https://doi.org/10.1093/mnras/stt2360)
- Walker, A. R. 1983, *South African Astronomical Observatory Circular*, 7
- Wenger, M., Ochsenein, F., Egret, D., et al. 2000, *A&AS*, 143, 9, doi: [10.1051/aas:2000332](https://doi.org/10.1051/aas:2000332)
- West, A. A., Weisenburger, K. L., Irwin, J., et al. 2015, *ApJ*, 812, 3, doi: [10.1088/0004-637X/812/1/3](https://doi.org/10.1088/0004-637X/812/1/3)
- White, R. J., Gabor, J. M., & Hillenbrand, L. A. 2007, *AJ*, 133, 2524, doi: [10.1086/514336](https://doi.org/10.1086/514336)
- Yuk, I.-S., Jaffe, D. T., Barnes, S., et al. 2010, in *Proc. SPIE*, Vol. 7735, Ground-based and Airborne Instrumentation for Astronomy III, 77351M
- Zuckerman, B., & Song, I. 2004, *ARA&A*, 42, 685, doi: [10.1146/annurev.astro.42.053102.134111](https://doi.org/10.1146/annurev.astro.42.053102.134111)